IRIS AperTO

UNIVERSITÀ DEGLI STUDI DI TORINO

AperTO - Archivio Istituzionale Open Access dell'Università di Torino

Effects of particle size on properties and thermal inertization of bottom ashes (MSW of Turin's incinerator)

This is the author's manuscript

Original Citation:

Availability:

This version is available http://hdl.handle.net/2318/1689835 since 2019-02-04T17:44:03Z

Published version:

DOI:10.1016/j.wasman.2018.11.050

Terms of use:

Open Access

Anyone can freely access the full text of works made available as "Open Access". Works made available under a Creative Commons license can be used according to the terms and conditions of said license. Use of all other works requires consent of the right holder (author or publisher) if not exempted from copyright protection by the applicable law.

(Article begins on next page)

31 October 2024

Effects of particle size on properties and thermal inertization of bottom ashes (MSW of Turin's incinerator)

Caterina Caviglia, Giorgia Confalonieria, Ingrid Corazzari, Enrico Destefanis, Giuseppe Mandrone, Linda Pastero, Renato Boero, Alessandro Pavese

Waste Management: 84 (2019) p 340-354 https://doi.org/10.1016/j.wasman.2018.11.050

Abstract

The aim of this study is twofold: (i) characterization of the bottom ashes from the Incinerator plant of the city of Turin (northern Italy), in terms of their chemical/phase compositions and capacity to release heavy metals in leachates, as a function of particle size; (ii) investigation of thermal treatments' efficacy to promote inertization of the same bottom ashes, exploring time-temperature ranges with $t \leq 6$ h and $T \leq 1000$ °C. Special attention is paid to macro-sampling techniques in order to have samples that are representative of the average bottom ashes production. Micro-XRF, ICP-OES, SEM-EDS, Ion Chromatography and X-ray powder diffraction were used to investigate bottom ashes and leachates. Bottom ashes are mainly constituted by an amorphous phase, ~66–97 wt%, regardless of particle size; the remaining phases are quartz, calcite, Fe-oxides, melilite and other minor crystalline materials. The amorphous phase exhibits a relevant dependence on particle size, and undergoes dissolution in water up to 20 wt%, thus being the most important component in affecting chemical species release. The smaller the bottom ashes' particle size, the more the heavy metals (major species: Zn, Cu, Ti, Pb) and calcium contents increase, whereas silicon's decreases. Electrolytic current observations in combination with phase/chemical composition and metals release as a function of particle size, suggest that bottom ashes partition into two classes, i.e. ≥1 and <1 mm, for inertization purposes. Thermal treatments exhibit partial efficacy to curb heavy metals mobility: whilst they reduce Cu release, they lead to a inverse effect in the case of Cr.

Keywords

Bottom ashesParticle size distributionLeachingHeavy metalsInertizationThermal treatments

1. Introduction

Municipal solid waste treatment technology has gained more and more importance during the last decade in developed and in development countries, especially in those with a high population density. Sustainable waste management is one of the most important targets even for the European Union and is being pursued through the implementation of community laws (Smol et al., 2015) and adoption of appropriate treatment methods to recover from waste a significant amount of material and energy. Incineration is a fundamental process to reduce the volumes of waste, but it produces fly and bottom ashes that must be disposed of. In 2014, around 88 million tons of waste (municipal, commercial and industrial) were treated in Waste-to-Energy plants in Europe: the incineration process produced approximately 18 million tons of bottom ashes (CEWEP, 2014). Bottom ashes (BA) are the solid residue produced by municipal solid waste incineration facilities, mainly constituted by unburnable and inert materials, and they represent about 21% of the weight of the material treated by the incinerators in Europe. BA are classified by the European Waste Catalogue as industrial non-hazardous wastes. After the European Council Regulation 2017/997 (European Union, 2017), MSWI bottom ashes could be classified as dangerous waste. The limits of concentration for many dangerous substances will be more restrictive, like for Zn and Cu oxides, whose concentration thresholds will be ten times lowered.

BA reuse is a common practice in many European (Belgium, Denmark, Netherlands, Germany, Spain etc.; CEWEP, 2006) and non-European countries as China, Taiwan and USA; Crillesen and Skaarup, 2006, Lam et

This is the authors copy of the original published in https://doi.org/10.1016/j.wasman.2018.11.050

al., 2010, Dou et al., 2017. Currently the main reuse applications of BA are: replacement of aggregates in concrete/mortars (Pan et al., 2008, Marinoni et al., 2009, Sorlini et al., 2011), material for roads construction (Eymael et al., 1994, Huang et al., 2006, De Windt et al., 2011, Shih and Ma, 2011), material for landfills, material for ceramic production, after a vitrification process (Cheeseman et al., 2003, Schabbach et al., 2012). In Denmark, around 99% of the BA produced in the incinerator plants of the country is being reused. The legislation has allowed the use of BA in road construction for many years, even for high load roads in 2012 (Hjelmar and Holm, 2007, Lynn et al., 2017). In the Netherlands and in Germany, aggregates from BA are also used in the construction of flyover for highways and noise barriers (Minane et al, 2017).

Before being used in any application, waste must undergo treatments to be stabilized and to avoid release of contaminants: washing and leaching processes (Lam et al., 2010); solidification/stabilization methods through additives (Quina et al., 2008); thermal treatments, like vitrification (Xiao et al., 2008); assisted carbonation (Van Gerven et al., 2005, Arickx et al., 2007).

In Italy, around 82 wt% of BA produced by incinerators was treated in 2016 for reuse and only 18% was landfilled. Statistical data of ISPRA – Institute for the Protection and Environmental Research (ISPRA, 2017, ISPRA, 2014) show differences which depend on the geographical areas: northern Italy recovers some 75,6 wt% of the bottom ashes, while central Italy only 8,4 wt%, and southern Italy about 15,9 wt%. Most of the recovered material is represented by additive for cement (97 wt%); the remaining is destined to ferrous and non-ferrous metals recovery (Riva et al., 2016) and to provide a base material for landfills (Puma et al., 2013). According to the Italian Legislation about reuse of waste (Decree n.186 of the 5th April 2006) BA can be reused without any treatment or acceptance test for the production of cement, bricks and expanded clay. In the case of road material, bottom ashes can be used if leaching tests comply with the thresholds provided for heavy metals (Lombardi and Carnevale, 2016).

In the BSB Plant of Noceto (Parma, Italy) gravels from BA are being crushed and used as aggregate for concrete manufacturing (Grosso et al., 2011). Bottom ashes are also tested successfully for reuse in ceramics after vitrification processes (Barbieri et al., 2000). In general, many efforts are being steered towards devising new approaches to treat and manage waste from incineration (Lothenbach et al., 2011, Miezah et al., 2015, Verbinnen et al., 2017, Toniolo and Boccaccini, 2017).

In the light of a growing attention to ashes from urban solid wastes incineration, it is becoming more and more important to investigate the properties of such materials in view of a possible fractionation into particle size sub-classes, to optimize their re-cycling and/or re-use, at as low costs as possible. A further difficulty arises from that ashes of incineration are sensitive to treatment plant technologies and seasonality, which reflects the nature of the collected garbage. Two approaches are being taken to tackle the variability of ashes: (1) large amounts of ashes from several plants are mixed, to attain an average material that reduces fluctuations; (2) attention is focused on large scale plants, to plan specific treatments and maximize the capacity of re-use/re-cycling of the produced waste. While the first approach is more convenient on an economic point of view, the second one is destined to become relevant, taking into account a general tendency to valorize at best ashes for technologies of growing complexity.

The present study focusses on the bottom ashes from the Incineration Plant of Turin (Northwestern Italy), which converts garbage into BA at a ratio of approximately 5:1. Our aim is to develop a highly efficient and low cost BA inertization technology specialized for such kind of waste. We consider “inertization” as a full cessation, or at minimum a cessation below legal thresholds, of environmentally dangerous species release (foremost heavy metals, sulfates and chlorides). The present investigation’s target is threefold:

(1)to provide a characterization of BA as a function of their particle size distribution (release kinetics and leaching behavior), so as to exploit features that are related to particle size fractionation;

This is the authors copy of the original published in https://doi.org/10.1016/j.wasman.2018.11.050

(2)to design possible new aggregations of the BA into particle size classes, which are functional to subsequent treatments for inertization;

(3)to test time-temperature (t-T) thermal treatments, over t-T ranges, which are economically/technically sustainable/feasible.

2. Material and methods

BA were sampled in the thermal-valorization plant of the city of Turin. The plant is working since 2014 and burns about 500.000 t of waste per year, with three lines of combustion, and a total capacity of 67,5 tons/h, at a firing peak temperature of some 1000 °C.

The scheme reported in Fig. 1 shows the general methodology followed to investigate our samples: sampling, subsampling, chemical and phase composition of BA, leaching properties in water and leaching kinetics of BA, re-aggregation of BA as a function of their particle size and eventually thermal treatments to test their efficacy to curb heavy metals release.

2.1. Sampling and subsampling

Bottom ashes were collected from a falling stream (Møller, 2004), for a total of ∼20 kg, thus obtaining a general sample. Each general sample was first homogenized by stirring; then, divided by mechanical quartering, using a riffle splitter (Gerlach et al., 2002, Petersen et al., 2005), to have representative subsamples, each one of ∼2 kg. A total of three representative subsamples were prepared. Two further 20 kg samplings were accomplished, following the same procedure, and their analyses are still in progress. Preliminary grain size determinations and leaching tests provide results that are fully comparable to those from the first sampling.

Each representative subsample was dried in an oven at 105 °C and then sift to determine the particle size distribution. The following opening standards were used: <0,063 mm, 0,063, 0,5, 1, 2, 4, 8, 16, 20 mm, according to the European standards for aggregates EN 933-2, and following Chimenos et al., 1999, Del Valle-Zermeño et al., 2017, save the addition of one class more for the finest fraction, i.e. <0,063 mm class. The samples under investigation are labelled by “QR X”, where QR and X mean “quartering” and grain size, respectively, the latter ranging from <0,063 to 20 mm. The surface area of the samples was measured by means of the BET method that exploits N2 adsorption at 77 K, by a ASAP 2010 surface area analyzer (Micromeritics, Norcross, GA, U.S.A).

2.2. Chemical and phase composition determination

Samples were ground into a fine powder using a mechanical mill with agate bowls, and then pressed at 1 ton/31,75 mm into pellets, to carry out chemical analyses, using X-Ray Fluorescence (XRF) and Scanning Electron Microscopy (SEM) in combination with Energy Dispersive Spectroscopy (EDS). More investigations on chemical composition were performed by Inductively Coupled Plasma–Optical Emission Spectrometry (ICP-OES) on microwave dissolved samples, using the EPA method 3051 A. Phase composition was determined by means of X-ray Powder Diffraction (XRPD).

2.2.1. XRF measurements

XRF measurements were performed by a μ-XRF Eagle IIIXPL with EDS Si(Li) 30 mm2 detector and analytic software Edax Vision32, on three subsamples to determine the elemental content of every particle size class from <0,063 to 20 mm. The following elements were revealed and quantified: Si, Ca, Al, Fe, P, S, Cl, K, Ti, V, Cr, Mn, Ni, Cu, Zn, As, Sr, Pb. The composition of every sample was determined as the average of an array of 9 × 9 analysis pixels, on a squared area of ∼7 × 7 mm; every pixel corresponds to 0,5 mm; the beam

This is the authors copy of the original published in https://doi.org/10.1016/j.wasman.2018.11.050

was defocused at ~165 μm spot diameter. The total number of spectra was 648, with 3 × 105 countings, 10 s per pixel recording. The uncertainty on the average values was estimated using the related standard deviation.

2.2.2. Dissolution by microwave (EPA method 3051 A)

Three subsamples were analyzed by ICP-OES (Perkin Elmer Optima 2000 DV), applying a calibration curve determined by four points using a Merck ICP multi-elements-standard solution IV. First, each sample was dissolved by microwave technique, using 0,1 g of fine powder for every particle size class from <20 to <0,063 mm and 10 mL of nitric acid. We used an Anton-Paar Multiwave 7000 digestion system to perform the dissolution process with microwave and no evaporation occurred. The resulting solutions were diluted with ultra-pure water, at a ratio of 1:3, and then analyzed.

2.2.3. SEM-EDS analyses

Secondary electrons (SE) imaging and back scattered electrons (BSE) analyses were performed by a Scanning Electron Microscope JSM IT300LV High Vacuum – Low Vacuum 10/650 Pa – 0.3–30 kV (JEOL USA Inc.), equipped with SE and BSE detectors (typical experimental conditions: W filament, EHT 15 kV, working distance 10 mm, high probe current). The following elements were revealed and measured: Al, Si, K, Ca, Na, Mg, S, Cl, P, Cr, Mn, Fe, Cu, Zn, Ti. The surface under investigation of a given sample was partitioned into 100 areas, and each one analyzed. The overall chemical composition and related uncertainty were estimated by the average and expected standard deviation of the measurements above, respectively.

2.2.4. Phase composition: X-ray powder diffraction

X-Ray Powder Diffraction data collections were performed by a PANalyticalX'Pert Pro Bragg Brentano (θ/2θ) diffractometer, whose instrument equipment and operating conditions are extensively reported elsewhere (Marinoni et al., 2017). Samples were rotated at 16 rprm and patterns were collected between 5° and 80° 2θ-angle, with a 2θ-step size of 0.017°. The amorphous phase quantification was carried out by combining Rietveld and reference intensity ratio (RIR) methods (Pagani et al., 2010, Gualtieri, 2000;). High purity calcined α-Al2O3 corundum was used as an internal standard and added to the ground samples (10 wt%). Data refinements were performed by the software GSASII (Toby and Von Dreele 2013).

2.3. Thermo-gravimetric analysis

Thermo-gravimetric analyses were carried out by an instrument TA Q200, using 20 mg of material (raw bottom ash) up to 1000 °C and heating ramp of 20 °C/min. To assess the nature and the amount of the species evolved during the heating, an ultra-microbalance (sensitivity 0.1 μg) connected with a time-resolved FTIR detector was employed. The experiment was carried out on two samples, differing the one from the other by the aggregate size (i.e grain size >1 mm and <1 mm). Approximately 10 mg of each sample were heated from 30 to 1000 °C at the rate of 20 °C min−1 under dynamic oxidizing atmosphere (O2/N2 1:3, flow rate: 35 mL min−1) in a Pyris 1 TGA (Perkin Elmer, Waltham, MA, USA). The gas evolved during the heating ramp was piped (gas flow 65 mL min−1) via a pressurized heated transfer line (Redshift S.r.l. e Vicenza, Italy) and analyzed continuously by the FTIR (Spectrum 100, Perkin Elmer), equipped with a thermostatic conventional gas cell. Temperature resolved spectra were acquired in the 4000–600 cm−1 wavenumber range with a resolution of 0.4 cm−1 and analyzed with the Spectrum software (Perkin Elmer) to identify the nature of volatiles. Infrared profiles of each single species desorbed from the samples were obtained from the intensity of a representative peak of the investigated species as a function of temperature.

2.4. Conductivity analyses method

This is the authors copy of the original published in https://doi.org/10.1016/j.wasman.2018.11.050

Electrolytic conductivity was recorded continuously using temperature and conductivity probes of ES-2 Decagon Devices type, for every samples of BA.

2.5. Leaching tests

Leaching tests were performed following the European standard for characterization of waste EN-12457-2 (leaching test in deionized water for particles with size <4 mm, and a ratio Liquid/Solid 10) and EN-12457-4 (leaching tests in deionized water for particles of size <10 mm, and a ratio L/S 10/1) (Lin et al., 2017, Yin et al., 2017).

Leaching experiments, whose full duration was set at 70–80 h, were carried out using 20 g of every particle size class (0,063, 0,5, 1, 2, 4, 8, 16, 20 mm), from two subsamples previously dried. Water content was estimated around 15% for the three subsamples without grain size discrimination. Thermo-gravimetric analyses carried on the two samples of BA (above and under 1 mm grain size) showed an overall mass loss of 2.7% and 12.8%, (see paragraph 3.1). Each leaching test was performed trice, and the average results are here used. In case of contradictory results, such procedure was repeated until achievement of an internally consistent set of measurements. Attention was paid to how particle morphology, exposed surface and contact time affect leaching, recording electrolyte conductivity versus time. Electrolytic conductivity can be related to the exposed surface size, as shown by that the fine grain particles (<1 mm size) exhibited higher conductivity as a function of time, than the coarse grain particles (≥1 mm size). This might be also associated to the higher disintegration of the material fraction constituted by fine particles, and its consequent larger solubilization.

After the leaching tests, the resulting solutions were filtered and analyzed by:

1) ICP-OES, to measure the concentrations of Al-Pb-Cu-Ni-Zn-Cr-Co-Cd-Sr-Ba-Zn-Fe-Ti;
2) Ion Chromatography, to re-determine and cross-check the major elements, and to measure species such as Cl−, SO42−, F−, NH4+, NO33−, NO2− and Br−, using a Metrohm 883 Basic IC plus instrument, a loop of 20 µl and a calibration by 8 analysis points on a reference sample;
3) Atomic Absorption Spectrometry, to measure Sb concentration, using a Perkin Elmer Analyst 600 spectrometer, equipped with a graphite furnace.

2.6. t-T Treatments

BA were treated by thermal heating as a function of time and temperature, to investigate how far the thermally induced transformations on bottom ashes' structure and composition affect elemental release in water. We used a Carbolite CWF 1100 muffle furnace and carried out treatments as long as 30, 60, 120 and 360 min, exploring a thermal range from 200 to 1000 °C. A heating ramp of 4 °C/min was used. Samples were cooled down by abrupt interruption of heating, keeping them in closed furnace up to 300 °C, and eventually letting them equilibrate with ambient in open air. After thermal treatments, the samples underwent full characterization, leaching tests and the solid residues were eventually analyzed via XRPD and XRF.

3. Results and discussion

The particle size distribution of BA lies in the typical range encompassing coarse sands and fine gravels (D50 = 4 mm). All the explored subsamples exhibit very similar particle size distributions and, in this light, we chose to use their average for further speculations. In Fig. 2 the cumulative particle size distributions of three subsamples are shown. Each point is calculated as follows: (Total weight − Retained weight)/Total weight × 100.

3.1. Phase and chemical composition of BA

This is the authors copy of the original published in https://doi.org/10.1016/j.wasman.2018.11.050

Results of quantitative phase analyses on the samples QR X, before and after leaching process, are set out in Table 1. The uncertainties on phase amounts from the Rietveld profile analysis are often underestimated. Moreover, the investigated BA samples reveal a large number of occurring phases, which are different from the ideal ones, in terms of both stoichiometry and crystal structure. In this light, it was chosen to round off uncertainties on crystalline phases' amounts to unity, in order to provide a more reliable estimation of the errors than bare e.s.ds from profile fitting do. Phase amounts smaller than unity were rounded off to 1 wt%. Uncertainties on the amorphous phase, in turn, were calculated by the propagations of errors using the uncertainties on the crystalline phases, as previously discussed. Despite large uncertainties on phase composition, general trends are observable and in keeping with chemical composition determinations by XRF+SEM-EDS+ICP-OES, thus confirming the reliability of the XRPD quantitative phase analyses.

Table 1. Results of the quantitative phase analysis for samples [QR 20 – QR 0.063] are reported before (pre) and after (post) leaching treatment. Hematite and magnetite are gathered under "Fe oxide".

		Amorphous	Quartz	Calcite	Feldspar	Cristobalite	Fe Oxide	Melilite	Halite	Aluminum
		(wt%)	(wt%)	(wt%)	(wt%)	(wt%)	(wt%)	(wt%)	(wt%)	(wt%)
QR 20	Pre	74(6)	14(1)	9(1)	3(1)					
QR 16	Pre	97(1)	1(1)	1(1)						1(1)
QR 10	Pre	67(7)	15(1)	16(1)	2(1)					
	Post	96(1)	4(1)							
QR 8	Pre	89(2)	5(1)		2(1)		1(1)	2(1)	1(1)	
	Post	80(3)	8(1)	4(1)	1(1)		1(1)	6(1)		
QR 4	Pre	83(8)	3(1)		3(1)	1(1)	2(1)	8(1)		
	Post	69(7)	17(1)		5(1)		5(1)	4(1)		
QR 2	Pre	85(3)	6(1)	2(1)	2(1)	1(1)	1(1)	2(1)	1(1)	
	Post	77(6)	11(1)	2(1)	4(1)		1(1)	5(1)		
QR 1	Pre	75(6)	11(1)	2(1)	6(1)	1(1)	2(1)	2(1)	1(1)	
	Post	77(8)	11(1)	3(1)	4(1)	1(1)	1(1)	3(1)		
QR 0,5	Pre	66(7)	15(1)	3(1)	8(1)	1(1)	3(1)	3(1)	1(1)	
	Post	74(6)	15(1)	2(1)	4(1)	1(1)	1(1)	3(1)		
QR 0,063	Pre	80(3)	8(1)	4(1)	3(1)		1(1)	3(1)	1(1)	
	Post	70(7)	13(1)	6(1)	8(1)		1(1)	2(1)		

The average phase composition of the bottom ashes, determined as the particle-size-distribution weighted average of the phase compositions from each grain size class, is represented by: 79 wt% amorphous; 8 wt%

This is the authors copy of the original published in https://doi.org/10.1016/j.wasman.2018.11.050

quartz, 4 wt% calcite, 3 wt% feldspar (plagioclase and K-feldspar), 5 wt% other phases. Other phases occur in terms of amounts rounded off at 1 wt% (i.e. Fe-Oxides, akermanite-gehlenite, halite, aluminum, cristobalite). The 1% threshold is reflective of a phase amounts re-scaling to smaller figures owing to the large content of amorphous phase, which thus implies a formal lowering of the detection limit. The relevant content of the amorphous phase indicates that BA represent the dominant output of an off-equilibrium thermal process and hints at a potentially high residual reactivity, which may lead to an intense chemical species exchange/release in water.

Before leaching (Table 1), all the BA particle size classes contain a large amount of amorphous phase (>70 wt%), accompanied by minor phases, i.e. quartz, calcite (except in QR8 and 4) and feldspar. Cristobalite, Fe-oxide (hematite or magnetite), melilite and halite were seen at a level of detectability threshold in samples with grain size smaller than 10 mm, whereas aluminum was found in the QR 16 sample only. The presence of crystalline phases as melilite proves the samples to have experienced high temperature, during the firing process of the waste or in previous production processes.

Comparison between mineralogical compositions before and after leaching is complex. In fact, a loss of ~15–20 wt% (monotonically decreasing from small to large particle size) is to be taken into account. Therefore, initial phases contents have to be rescaled to be compared with those after leaching. Simulations were performed to find the scheme which best accounts for such weight loss. Comparison between calculations and results obtained by the Rietveld analysis on solid residue suggests to ascribe the observed mass reduction to the amorphous phase dissolution. This is also in agreement with the fact that the most of the minor crystalline phases are not easily dissolvable by the used leaching process. In Fig. 3, initial phase compositions (rescaled as discussed above) and those after leaching are shown, from Rietveld analysis. Crystalline phases are modestly affected by leaching, bar halite, which completely dissolves into solution (Table 1).

An anomalous behavior is revealed by QR10, wherein the amorphous phase increases after leaching. Leaching and measurements were repeated, using the same sample, but the results remained substantially unchanged. We are cautious to maintain this to represent an actual feature of the QR10 class. Such an anomaly could be tentatively ascribed to a casual concentration of low crystallinity materials, which underwent either amorphization or dissolution, possibly followed by the precipitation into a glass phase.

Chemical composition of BA was determined by combining data from μ-XRF, SEM-EDS and ICP-OES. The observed chemical species are Si, Ca, Al, Fe, P, S, Cl, K, Ti, V, Cr, Mn, Ni, Cu, Zn, As, Sr and Pb, as reported in Tables 2a, b, in terms of elemental molar percentages. Si, Ca, Al, Fe, Mg, Na and K (in order of abundance) are the major occurring species, along with Cl, P and S. The highest concentrations of heavy metals, save iron, are due to Cr, Ti, Zn and Cu (Jung et al., 2004). Fig. 4 shows such elements' abundances as a function of grain size. Si decreases upon decreasing grain size, while Ca increases. This behavior is mainly attributable to the amorphous phase's composition, which remarkably changes as a function of particle size, as discussed below. The other elements do not exhibit a so well-defined correlation between their abundance and particle size. However, heavy metals like Pb, Ni and Ti tend to concentrate in the fine grain sizes, while Cr and Cu exhibit a preference for the coarse ones (Fig. 4), altogether.

Table 2. a and b. Molar composition of BA as function of the particle size (mm), and average composition (mol %).

This is the authors copy of the original published in https://doi.org/10.1016/j.wasman.2018.11.050

Grain size (mm)	Na	Mg	Si	Ca	Al	Fe	P	S	Cl	K
20	0.039	0.020	0.510	0.093	0.044	0.035	0.013	0.011	0.001	0.005
16	0.009	0.007	0.193	0.025	0.023	0.009	0.005	0.002	0.000	0.002
10	0.038	0.042	0.503	0.149	0.060	0.079	0.026	0.051	0.007	0.004
8	0.042	0.025	0.460	0.109	0.053	0.050	0.023	0.014	0.003	0.005
4	0.085	0.057	0.854	0.332	0.090	0.056	0.051	0.093	0.012	0.011
2	0.040	0.067	0.699	0.196	0.099	0.094	0.050	0.034	0.006	0.009
1	0.034	0.056	0.616	0.204	0.101	0.090	0.048	0.042	0.008	0.010
0.5	0.017	0.024	0.307	0.104	0.046	0.052	0.030	0.026	0.004	0.005
0.063	0.023	0.028	0.279	0.198	0.059	0.039	0.047	0.071	0.012	0.007
<0,063	0.009	0.010	0.083	0.077	0.020	0.012	0.014	0.029	0.004	0.002
average	0.336	0.334	4.503	1.486	0.596	0.516	0.307	0.373	0.056	0.059
average comp.(%)	3.836	3.816	51.422	16.973	6.807	5.887	3.505	4.255	0.645	0.672

Grain size (mm)	Ti	Cr	Mn	Ni	Cu	Zn	Sr	Pb
20	4.78E−03	2.73E−03	6.40E−04	6.03E−05	2.43E−03	4.74E−04	1.98E−04	2.84E−05
16	2.79E−03	3.17E−04	3.00E−04	1.79E−05	1.36E−04	1.39E−04	6.10E−05	8.19E−06
10	9.95E−03	1.13E−03	1.50E−03	1.20E−04	1.37E−03	1.50E−03	2.61E−04	3.33E−05
8	7.37E−03	1.15E−03	8.86E−04	7.13E−05	3.98E−03	1.27E−02	2.55E−04	2.57E−05
4	2.16E−02	2.44E−03	2.16E−03	2.42E−04	1.71E−03	2.80E−03	5.16E−04	2.71E−04
2	1.73E−02	1.86E−03	1.90E−03	1.29E−04	5.77E−03	4.09E−03	4.84E−04	6.86E−05
1	1.81E−02	1.93E−03	2.14E−03	1.43E−04	1.98E−03	3.26E−03	3.60E−04	6.35E−05
0.5	8.59E−03	8.85E−04	9.46E−04	7.46E−05	1.05E−03	1.43E−03	1.79E−04	4.20E−05
0.063	1.50E−02	1.29E−03	1.27E−03	1.48E−04	1.33E−03	2.71E−03	2.83E−04	6.39E−05
<0,063	4.66E−03	4.25E−04	4.51E−04	7.20E−05	4.50E−04	8.88E−04	1.06E−04	2.53E−05
average	1.10E−01	1.42E−02	1.22E−02	1.08E−03	2.02E−02	3.00E−02	2.70E−03	6.30E−04
average comp.(%)	1.26E+00	1.62E−01	1.39E−01	1.23E−02	2.31E−01	3.43E−01	3.09E−02	7.19E−03

Table 2c. Mass loss from TGA analysis (wt %), TOC (mg/l) and BET analysis (m2/g) of the two fractions of BA ≥ 1 mm and <1 mm.

Grain size	Mass loss % (TGA)	TOC (mg/l)	BET (m2/g)
≥1 mm	2.7	28.54	5.6
<1 mm	12.8	116.9	10.5

This is the authors copy of the original published in https://doi.org/10.1016/j.wasman.2018.11.050

Results from thermo-gravimetric analyses on total BA are displayed by Fig. 5. Weight loss exhibits three ranges as a function of T: (i) a moderate weight loss at ∼100 °C (ascribable to surface water loss); (ii) a weight loss of some 5–6 wt%, over the range 300–600 °C; (iii) a weight loss, of 1–2 wt%, in the interval 850–900 °C. The 300–600 °C reaction is likely due to transformations involving microcrystalline carbonate (decarbonation) phases and plastic combustion residue (molecular decomposition), as suggested by visual observations on BA, which revealed the occurrence of not-fully burnt plastic fragments.

To assess the nature of the degradative processes induced by the heating under oxidizing atmosphere, TGA coupled with FTIR analysis of the gas evolved during the heating was carried out on two fractions of BA: grain >1 mm (sample 1) and grain <1 mm (sample 2). The results obtained are reported in Fig. 6. Sample 1 and sample 2 exhibited an overall mass loss of 2.7% and 12.8%, respectively. At lower temperature (30–200 °C) both the samples underwent a first thermal process (identified by the minimum at ca. 120 °C on the D-TG curve) which caused a weight loss of 0.7% for sample 1 and 2.5% for sample 2 due to the desorption of physi- and chemisorbed H2O as evidenced by FTIR. The different amounts of desorbed water can be ascribed to the different surface area exposed. At higher temperature (>200 °C), a complex series of partially superimposed processes took place. The thermal behavior of sample 1 was characterized by four different events, identified by the minima on the D-TG at ca. 260 °C, 360 °C, 490 °C, and 630 °C, which caused a total weight loss of 2% with the release of CO2 and H2O. These weight losses are consistent with degradation/oxidation of the residual organic fraction. The weight stabilized at ca. 700 °C. The behavior of sample 2 was characterized by five thermal degradations, which caused a weight loss of ca. 10.3%. The first four events are analogue to those observed with sample 1 and also in this case they can be assigned to oxidative degradation of organic species. In addition, a fifth process (ca. 700 °C on the D-TG curve) characterized by the evolution of CO2, which is assignable to the degradation of carbonates, was observed. Sample 2 differs from sample 1 by a higher amount of organic fraction and the presence of carbonates. Moreover, being the residual weight 97.3% for sample 1 and 87.2% for sample 2 evidences that the main component of both the samples was represented by ashes.

In view of the results from thermo-gravimetry, we can state that most of the amorphous phase is of inorganic origin, given that the organic fraction amounts to a maximum of 5 wt% out of a total contribution to the phase composition of 70–80 wt% (Table 1).

The chemical composition of the amorphous phase (Table 3a and b) was estimated by subtracting the contribution of the main crystalline phases (quartz, calcite, plagioclase, Fe-oxides, melilite and halite) from the total chemical composition of BA, as a function of grain size. The chemical composition of the amorphous phase for each particle size class is set out in Tables 3a and b, and results in the following formula unit:

where ξ(j) is the coefficient of the jth-element, choosing a normalization to 6 anions. Note that we neglected F and C, because the former is remarkably less abundant than Cl, and the latter is foremost attributable to either carbonate phases or plastic residues.

Table 3. a and b. Amorphous phase composition (mol) as function of the particle size; in table 3 b the composition is also reported as the sum of Na + K, Mg + Ca + Fe, Si + Al, P + S and transition elements (main heavy metals).

This is the authors copy of the original published in https://doi.org/10.1016/j.wasman.2018.11.050

Grain size (mm)	Na	Mg	Si	Ca	Al	Fe	P	S	K	Ti	Mn
20	19.23	5.09	36.11	20.02	6.92	5.98	1.32	0.97	2.32	0.62	0.11
16	14.44	5.46	39.87	16.62	12.04	4.38	1.44	0.62	3.16	1.07	0.15
10	13.90	6.13	29.98	25.14	6.85	9.62	1.91	3.13	1.49	0.91	0.18
8	16.89	5.12	36.15	22.25	6.29	6.19	1.87	0.93	2.11	0.75	0.12
4	15.72	5.47	33.17	31.79	2.72	2.27	1.97	2.96	2.06	1.03	0.14
2	9.86	8.75	31.87	25.07	7.40	7.58	2.65	1.50	2.44	1.14	0.17
1	9.46	8.21	28.01	29.11	7.91	6.98	2.80	2.07	2.86	1.33	0.21
0.5	9.66	7.31	26.05	30.45	6.39	8.23	3.69	2.64	3.01	1.32	0.19
0.063	10.51	6.38	10.66	43.98	7.20	5.24	4.35	5.44	3.02	1.73	0.20
<0,063	12.00	6.44	5.77	48.69	7.23	4.44	3.69	6.28	2.48	1.54	0.20

Grain size (mm)	Cr	Ni	Cu	Zn	Sr	Pb	Na+K	Mg+Ca+Fe	Si+Al	P+S	Transition elements
20	0.47	0.03	0.63	0.12	0.05	0.01	21.56	31.10	43.03	2.29	2.03
16	0.16	0.03	0.37	0.11	0.05	0.01	17.61	26.47	51.91	2.06	1.95
10	0.14	0.04	0.25	0.28	0.05	0.01	15.39	40.89	36.83	5.04	1.86
8	0.16	0.03	0.81	0.28	0.05	0.01	19.00	33.56	42.44	2.80	2.21
4	0.16	0.05	0.16	0.27	0.05	0.03	17.78	39.52	35.89	4.93	1.88
2	0.16	0.03	0.76	0.54	0.06	0.01	12.30	41.40	39.27	4.15	2.87
1	0.19	0.04	0.29	0.48	0.05	0.01	12.31	44.30	35.92	4.87	2.60
0.5	0.18	0.05	0.32	0.44	0.05	0.01	12.66	46.00	32.44	6.33	2.56
0.063	0.20	0.07	0.31	0.63	0.07	0.01	13.53	55.60	17.87	9.79	3.21
<0,063	0.19	0.10	0.30	0.59	0.07	0.02	14.48	59.57	12.99	9.97	2.99

In Table 3b and Fig. 7a and b, we show some aggregate compositions of the amorphous phase, as a function of particle size. Two main regions can be discriminated: one above and the other below 1 mm particle size. For BA < 1 mm, the composition of the amorphous phase is sensitive to the particle size, in particular as to Mg + Fe + Ca and Si + Al, whereas composition stabilizes for larger grain size. Small grain size BA's amorphous phase exhibit a composition suggesting a comparatively modest structural networking, owing to a reduction of Si + Al species that act as network formers in glasses (Bernasconi et al, 2018). Conversely, upon increasing particle size, Si + Al content allows formation of an amorphous phase that has, in principle, a potential capacity to develop towards ceramic glass or silicate crystal structures, if duly activated by thermal energy. Heavy metals show the trend mentioned above for total BA, that is Cu and Cr prefer large particle size, whilst the other transition elements exhibit a reverse behavior. Transmission electron microscopy observations might help shed light on elemental segregation and/or local partial crystallization occurring in the amorphous phase's disordered structure. All this hints that particle size is a critical parameter to discriminate BA, in terms of their general behavior. We expect significantly different exchanging properties in leaching treatments, between BA ≥ 1 mm and BA < 1 mm.

3.2. Leaching of bottom ashes

Fig. 8 shows electrolytic conductivity of the leaching solutions as a function of time, thus providing a depiction of the exchange/dissolution reaction kinetics. In keeping with the section above, two grain size ranges can be recognized, separated by a gap at 1 mm particle size: the fine grain size samples (0,5, and 0,05 mm), at the top of the diagram, show high conductivity values, which surpass by 6–10 times those due to the coarse grain size samples (from 1 to 16 mm). The conductivity of the grain size <0,063 is not reported

This is the authors copy of the original published in https://doi.org/10.1016/j.wasman.2018.11.050

in Fig. 8 for scale convenience. pH values, which show no significant changes upon time, lie around 10.5 and 11.5 for the grain size ≥1 mm and <1 mm, respectively.

Released heavy metals such as Zn, Cu, Ni and Pb, occur in higher concentrations in the leachates from fine grain size classes than in those from the coarse grain size ashes (Fig. 9). Only Cu lies above the legal threshold values, (0,05 mg/l), settled by the European Legislations 91/156/EEC and 91/698/EEC, and transposed into the Italian law about "not dangerous waste reuse", D.M. 5/04/2006 n.186, (Ministero dell'Ambiente e della Tutela del Territorio, 2006). Pb, Cu, Ni and Zn decrease upon decreasing the grain size. Cr, Co, Cd, Ba and Zn turn out to lie below the legal threshold values. In the Fig. 9, thresholds for Pb, Cu, Ni, Cr are shown as dashed lines. This behavior is in keeping with our previous observations related to: Fig. 10

(i) a dominant role of the amorphous phase, whose composition and tendency to dissolving depend on particle size;
(ii) a concentration of heavy metals in such a phase.

Sb leachates analyses have been performed on both individual grain size fractions and aggregate fractions, i.e. ≥1 mm and <1 mm. Measurements give concentrations that are higher in the fine fractions (0,07–0,01 mg/l) than in the coarse fractions (under 0,003 mg/l). In both cases, concentrations are under the European threshold limits for BA reuse for civil applications (Van Caneghem et al., 2016, Cornelis et al., 2006).

In general, Sb values measured on the BA samples taken for periodic monitoring, have always shown very low values, in contrast with flying ashes, from the same plant, which exhibit not negligible antimony figures.

3.3. Classification of BA into "fine" and "coarse" grain size classes

We chose to split BA into two classes, as a function of their particle size: BA-fine, <1 mm, and BA-coarse, ≥1 mm, on the basis of:

1) heavy metals release capacity versus grain size, whereby the estimated weighted sum (according to the cumulative particle size distribution of Fig. 2) of heavy metals concentrations in leachates of grain size <1 mm (∼3,3 mg/l) is more than three times larger than the one of grain size ≥1 mm (∼1,0 mg/l);
2) chemical composition of the major amorphous phase versus grain size (Fig. 7a and b), which exhibits an apparent dependence on particle size and provides a relevant contribution to electrolytes.

The leaching tests substantiate the difference of the conductivity trends between the BA-classes of grain size ≥1 mm and <1 mm, as shown in the conductivity/time diagram displayed by Fig. 8. BA-fine exhibit, as expected, remarkably higher electrolytic conductivity values than BA-coarse. This can be attributable to the BA-fine's larger surface exposed to leaching, leading to higher concentrations in solution of Na+, Ca2+, Cl− and SO42− than BA-coarse. BET analysis carried out on the two fractions of BA show that the grain size class <1 mm has a specific surface value double than the grain size class ≥1 mm (10,5 and 5,6 m2/g, respectively), see Table 2c. Note that the amounts of heavy metals like Pb, Zn, Cu and Ni are also related to the solutions' pH-values: the larger pH, the smaller is the solubility of the heavy metal ions, or salts, in water. The large pH-figures we measured are attributed to leaching involving alkalis, as suggested by Shim et al. (2003). Altogether, our observations agree with those of the mentioned authors, who report that the BA exchanging capacity of heavy metals increases upon decreasing bottom ashes particle size.

This is the authors copy of the original published in https://doi.org/10.1016/j.wasman.2018.11.050

Altogether, aggregate fractions have been restricted to the two chosen classes only given that they exhibit the sharpest differences among other possible aggregations, thus requiring the most different processing approaches for inertization and treatment, in general. All this results, too, in a relevant processing simplification, in view of wholesale industrial applications.

3.4. Heating treatments on the BA grain size classes ≥1 mm and <1 mm

Thermal treatments were applied only to the grain size ≥1 mm and <1 mm of bottom ashes, choosing t-T values of 0.5, 1, 3, 6 h and 200, 400, 700, 1000 °C. In Fig. 11, only the highest/lowest explored temperatures are reported, namely the series at 200 and 1000 °C.

Leaching tests on the thermally treated BA lead to pH figures that remain steady during measurements and lie in the range 10–10.5, for the particle size ≥1 mm, and 11–11.5, for the particle size <1 mm.

Conductivity values are high for BA with grain size <1 mm (3000–5000 μS/cm), and generally below, or in a few cases slightly higher than, 1000 μS/cm, for grain size ≥1 mm.

The very high conductivity values of the BA fine fraction are associated to a larger exchanging surface with respect to the coarse fraction. Fig. 11 proves that, in general, conductivity decreases as the treatment temperature and/or time increase. This behavior is reflective of a kinetic effect, affecting (i) decomposition upon heating of organic substances that may complex heavy metals and easily dissolve giving electrolytes (Arickx et al., 2007, Van Gerven et al., 2004) and (ii) increase of crystallinity degree that reduces the solubility of the solid systems.

The ICP-OES analyses of the leachates from thermally treated BA focus on Pb, Cu, Zn, Cr, Ba, Al, Ni, Fe and Ga (Chimenos et al., 1999, Van Gerven et al., 2005, Tsakalou et al., 2018). A substantial decrease of Pb, Cu and Zn concentration is observable as the temperature changes from 200 °C to 1000 °C (Pb: from 0,01 mg/to 0,0001 mg/l, −99%; Cu: from 2,3 mg/l to 0,0005 mg/l, −99%; Zn: from 0,03 to 0,002 mg/l, −93%), in agreement with Arickx et al (2007). Ni shows a decrease of −47% from 0,04 to 0,021 mg/l. Conversely, Cr, Ba and Al exhibit concentrations that increase by two order of magnitude for Cr and Ba (from 0,05 to 8,4 mg/l; from 0,04 to 1,13 mg/l), and of one order for Al (from 20 to 117 mg/l, 82%). Fe, Ni and Ga remain rather steady, showing some 15% of increase upon rising treatment temperature. Treatment time plays an important role in the case of comparatively low treatment temperatures (for instance, at 200 °C, conductivity changes by 20% as the time increases from 3 to 6 h), whereas it is secondary with respect to T > 400 °C (for instance, at 700 °C, conductivity changes by 0,03% at different treatment durations). However, In the case of Cu, treatment time has a relevant effect in decreasing its concentration: at 700 °C, 6 h of treatment reduce the concentration of Cu in the leachate from 0,01 to 0,003 mg/l, with respect to 1 h at the same temperature. Fig. 12a–f display Cr, Al and Cu concentrations as a function of t-T, by way of example. The phenomenology of heavy metals release after thermal treatment is difficult to be univocally explained and represents the effect of the combination of several causes, in addition to a complex chemical equilibrium involving dissolution reactions, mainly due to the amorphous phase. The increase of Cr, Fe, Ni and Al release might be related, in part, to a sublimation upon heating of a carbon-rich padding between grains, which acts as a cement and a barrier to exchanging. A visual qualitative observation on untreated and treated BA confirms the occurrence and progressive disappearance of such C-padding, as additionally demonstrated by TOC measurements. The relevant role of Cu, Pb and Zn organic complexes is claimed by Arickx et al.(2007). Fulvic acid-like compounds were found to be responsible for enhanced Cu leaching, through formation of highly soluble organic-copper complexes. Volatilization of organic matter because of heating makes Cu able no more to form organic-copper complexes (Van Gerven et al., 2004). Total organic carbon (TOC) analyses on the two untreated samples (≥1 mm and < 1 mm) of BA gave values of 28,54 mg/l and 116,9 mg/l (see Table 2c), respectively. In the three thermally treated samples (grain size <1 mm: 200 °C/3h, 400 °C/3 h, 700C°/3h, and 1000 °C/0,5h) TOC content is detectable only in the sample at

This is the authors copy of the original published in https://doi.org/10.1016/j.wasman.2018.11.050

200 °C/3 h, with a concentration of 194 mg C/l, in keeping with Cu2+ concentration decreasing in leachates at treatment temperature above 200 °C.

Moreover, Cu is likely to be trapped, at temperature over 400 °C, in the crystalline structure of tenorite, CuO (Hyks et al., 2010, Astrup et al., 2005, Grygar et al., 2004). Tenorite is weakly soluble in water at pH of 10–12, and gives a log m°Cu (expressed as mol/kg) lying between −6 and −8 mol/kg H2O (Palmer et al., 2005). Note that tenorite forms at some 300–400 °C (Grygar et al., 2004). At 400 °C, thermal treatment induces a Cu concentration reduction of an order of magnitude (Fig. 12e and f) with respect to heating at 200 °C. Cr, on the contrary, increases consistently in the leaching solutions upon thermal treatment. Such a behavior has been reported by other authors, too, and ascribed to either a reaction with metallic aluminum (Astrup et al., 2005, Hyks et al., 2010), or formation of calcium chromate (VI), from Cr(OH)3 (III) and Ca(OH)2 (appearance at around 300 and 700 °C; Matsuzawa et al., 2006). With reference to the Italian legal limits of elemental concentrations for waste reuse, Cr lies above the threshold (0,05 mg/l) in any treated sample; Cu surpasses the limit (0,05 mg/l) in the case of low treatment temperatures (≤200 °C), only; Pb and Zn fall below the limit values at any treatment temperature, and for untreated BA, too.

X-Ray diffraction measurements on ≥1 mm (Fig. 13a) and <1 mm (Fig. 13b) thermally treated BA show that the amorphous phase is still the main constituent, followed by quartz, feldspar, calcite and Fe oxide. No new crystal phase formation reveals in thermally treated samples with respect to untreated ones, and calcite disappears over 400 °C in the grain size <1 mm, i.e. at a lower temperature than the expected one because of the small carbonate's particle size. All this proves the need to use higher temperatures to promote partial crystallization of the amorphous phase, in addition to the observed sintering reactions at the interface between particles.

4. Conclusions

Bottom ashes from the Incinerator Plant of Turin have been investigated, and the results lead to the following conclusions:

• BA exhibit a particle size distribution consistent with those commonly observed in the range from coarse sands to fine gravels (D50 = 4 mm). About 70 wt% BA lie above 1 mm grain size;

• BA show a relevant dependence on particle size as far as Si, Ca and heavy metals concentration are concerned. Si decreases upon decreasing grain size, whereas Ca exhibits a reverse trend. Altogether, heavy metals concentration tends to increase in small size BA. The average molar composition (mol %) of BA is given by 52% Si, 17% Ca, 7% Al, 6% Fe, 4% Na and Mg. The highest concentrations of heavy metals (mol %) are observed for Ti (1,3%), Zn (0,3%), Cu (0,2%) and Cr (0,2%);

• Every particle size class shows a phase composition characterized by a major amorphous phase (>70 wt%), along with minor crystalline phases, such as quartz, calcite and feldspar, in agreement with previous investigations (Le et al., 2018, Bethanis et al., 2002, Eusden et al., 1999). Cristobalite, Fe oxide (hematite and/or magnetite), melilite and halite were found as much as 5 wt% in total. Unburnt/partially burnt materials occur as much as some 3–4 wt%. The amorphous phase chemical composition depends on the particle size: Si + Al concentrate in large size particles, whilst Mg + Fe + Ca prefer to enter small size BA; P + S show an increase in the small particle size, especially over the range 0,063–1 mm. Indeed, in the coarse grain fractions bottle glass waste occurs, as proven by macroscopic observations. Therefore, a part of amorphous phase in the coarse grain size fractions (>1 mm) can be attributable to the presence of such refuse glass, as mentioned by Del Valle-Zermeño et al. (2017). Comparing the amorphous phase's composition of BA coarse classes to the one of the average soda-lime glass (Marinoni et al., 2017, Marinoni et al., 2013) brings to light (i) a general agreement as to Si and Na contents and (ii) larger Ca, Mg, Al

This is the authors copy of the original published in https://doi.org/10.1016/j.wasman.2018.11.050

amounts in BA. All this hints that the larger the particle size, the more the amorphous phase tends to be structurally governed by network forming species, thus approaching somewhat a glass-like system that under vitrification conditions might develop towards ceramic glass;

• Grain size distribution and overall phase composition agree those from previous studies on bottom ashes (Izquierdo et al., 2002, Chimenos et al., 2003, Forteza et al., 2004). Heavy metals concentrate in fractions <1 mm, in keeping with earlier works (Xia et al., 2017, Chen et al., 2008, Chimenos et al., 2003).

• leaching treatments lead to an average mass decrease of ∼15–20 %wt of the solid, according to the trend that the larger the particle size, the smaller the weight loss. Such weight loss takes place foremost at the expense of the amorphous phase, which therefore largely affects electrolytic current and chemical species in solution;

• electrolytic conductivity observations in combination with chemical composition determination of BA suggest to split bottom ashes into two classes, i.e. ≥1 mm and <1 mm. The former exhibits: electrolytic conductivity (<1000 μS/cm), pH ∼10–10.5, lower concentrations of Cl− (<800 mg/l), Na+ (<500 mg/l) The latter yields: electrolytic conductivity up to 4000 μS/cm), pH ∼11–11.5, higher concentrations of Cl− (up to 1800 mg/l), Na+ (up to 950 mg/l). Moreover the sum of the heavy metals concentrations in the leachates of BA < 1 mm is more than three times larger than the one in the case of grain size ≥1 mm. Sb is always under the European legislation thresholds;

• thermal treatments on ≥1 mm and <1 mm are only partially effective to inhibit heavy metals mobility. In fact, Cu concentration in solution decreases owing to high temperature treatments. Cr and Al, on the contrary, increase their concentrations. With reference to the concentration thresholds for waste reuse, Cr and Ni are above the limits (0,05 and 0,001 mg/l, respectively). Cu lies above the limit value (0,05 mg/l) for low treatment temperatures (≥200 °C), only. Pb, Cd and Zn fall below the limit values, in the case of both treated and untreated BA. The reasons for such behaviors are many, and more than one cause affects heavy metals release: degree of crystallinity, occurrence of organic complexes, carbon film on grains.

Altogether, the present work underlines the importance to exploit the particle size dependence of bottom ashes' behavior, in view of designing possible new aggregations. All this is meant to promote technological advancements in treatments destined to BA full/partial inertization and re-use. Our results suggest a grain size separation at 1 mm, relying upon electrolytic and exchanging/release activities. Given that most chemical species exchanging activity is affected by the amorphous phase, it is necessary to engender its vitrification or decomposition into stable oxides. Thermal treatments, at t-T conditions that are economically feasible, do not suffice to fully activate such transformations, although they prove to be effective to partially curb heavy metals release.

Acknowledgements

AP is grateful to the Earths Sciences Department of the University of Milan for providing access to the XRPD facility to collect data that were here used to determine the phase compositions of the investigated samples.

This is the authors copy of the original published in https://doi.org/10.1016/j.wasman.2018.11.050

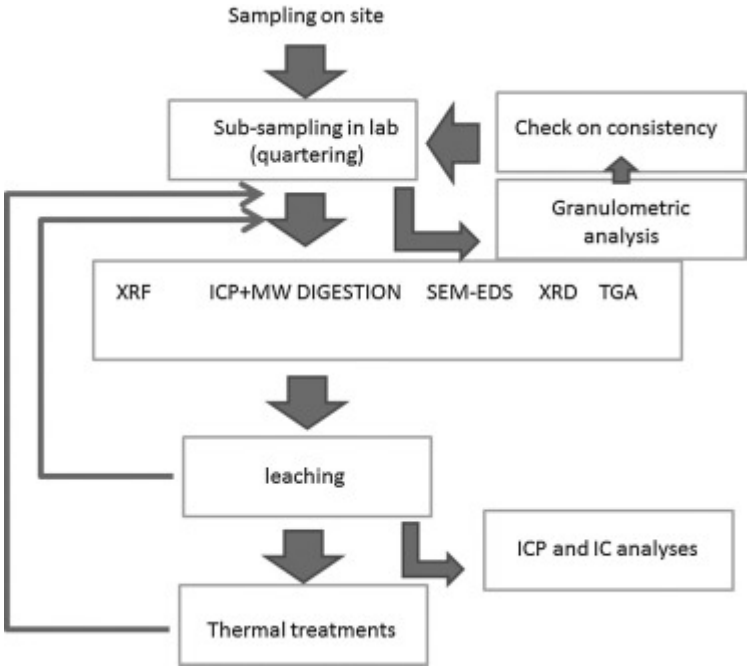

Fig. 1. Flow-chart of the analytical methodology followed in the present study.

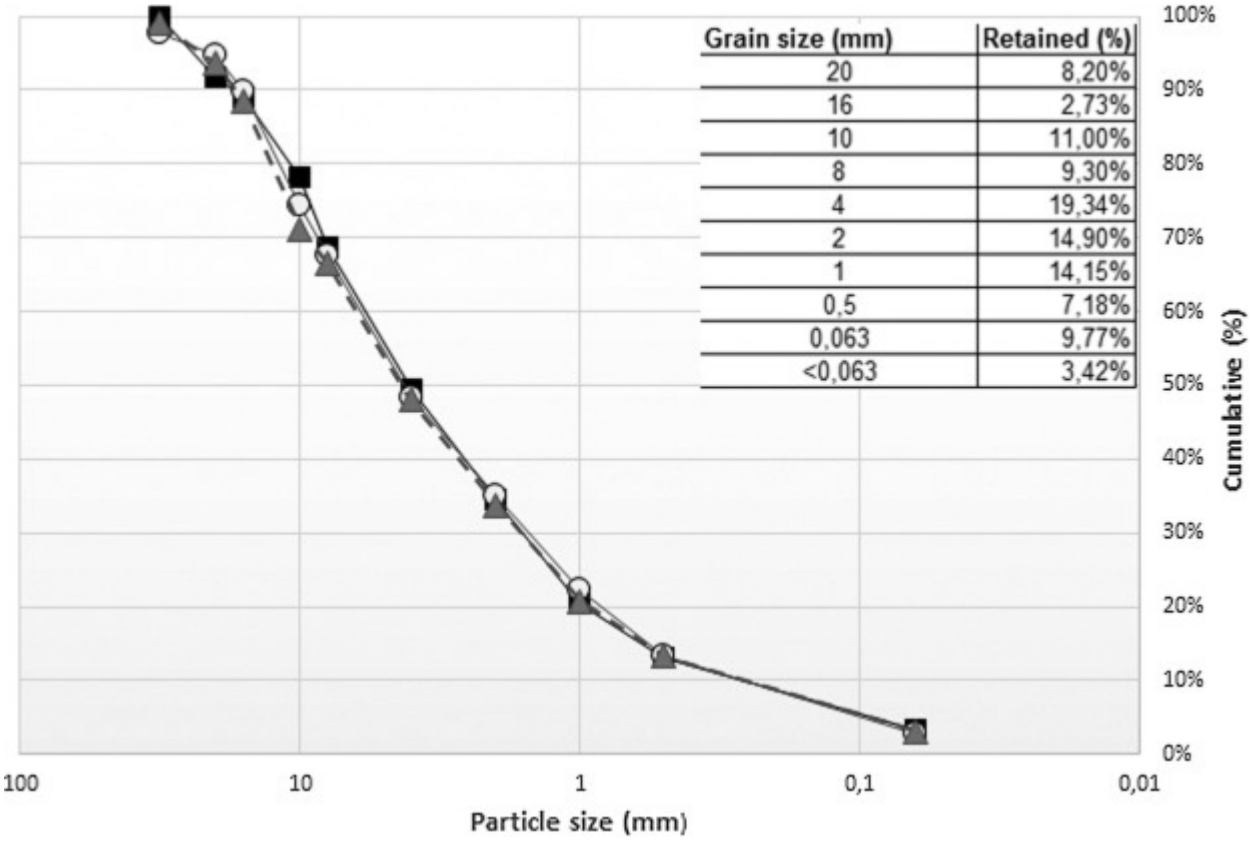

Fig. 2. Cumulative particle size distribution of three bottom ashes' subsamples. Solid line, dashed and dot-dashed lines are shown by way of example to demonstrate the high level of measurement reproducibility. The values in table are the average percentage of BA retained by every grain size class.

This is the authors copy of the original published in https://doi.org/10.1016/j.wasman.2018.11.050

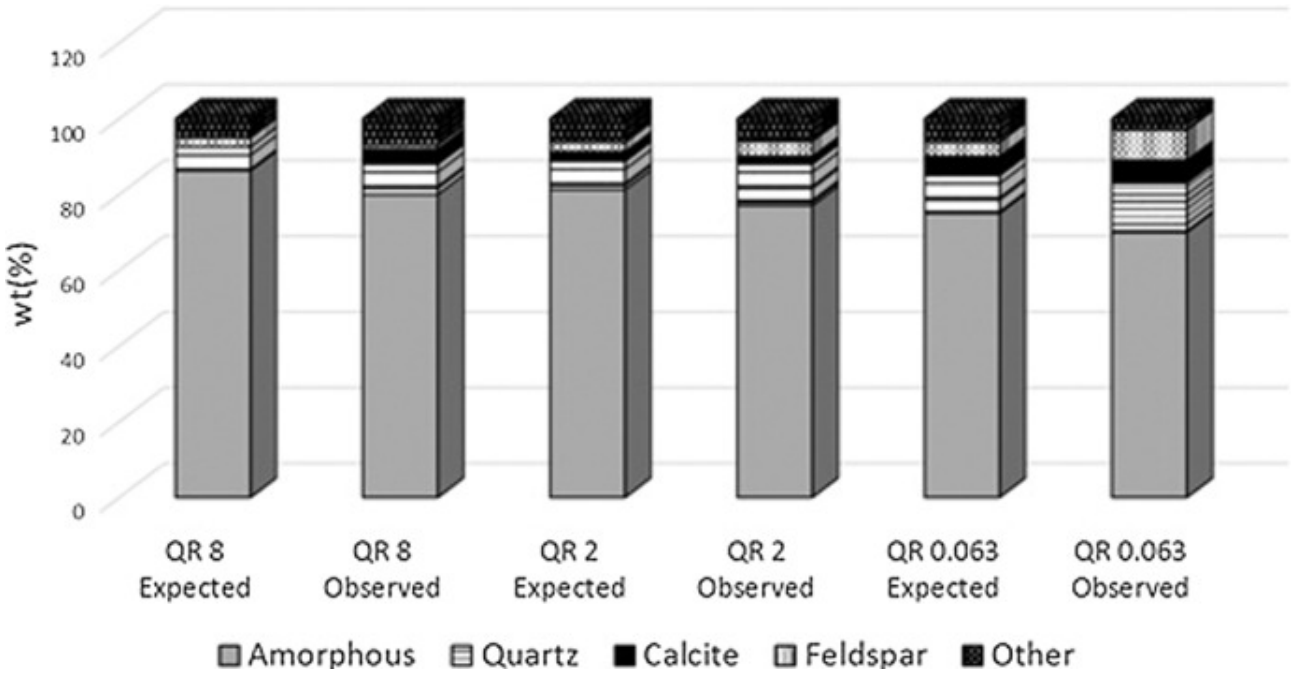

Fig. 3. Three examples of comparison between BA's expected phase compositions (from calculations, taking into account some 15–20% of weight loss at the expenses of the amorphous phase) and the observed ones, after leaching treatment.

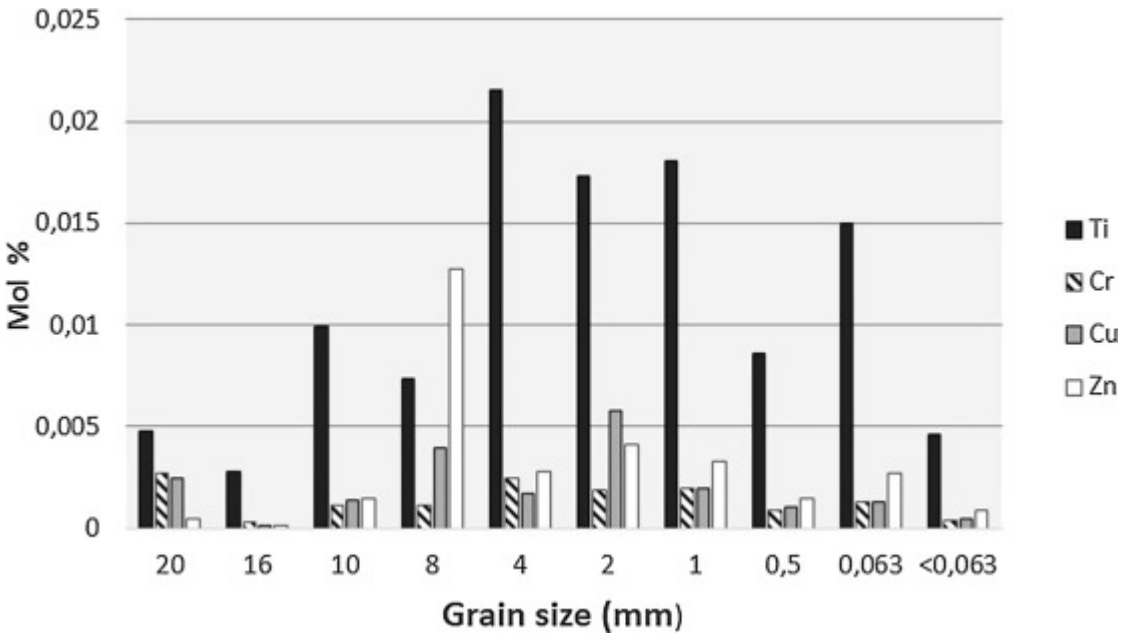

Fig. 4. Overall heavy metals molar percentage in BA, as a function of grain size.

This is the authors copy of the original published in https://doi.org/10.1016/j.wasman.2018.11.050

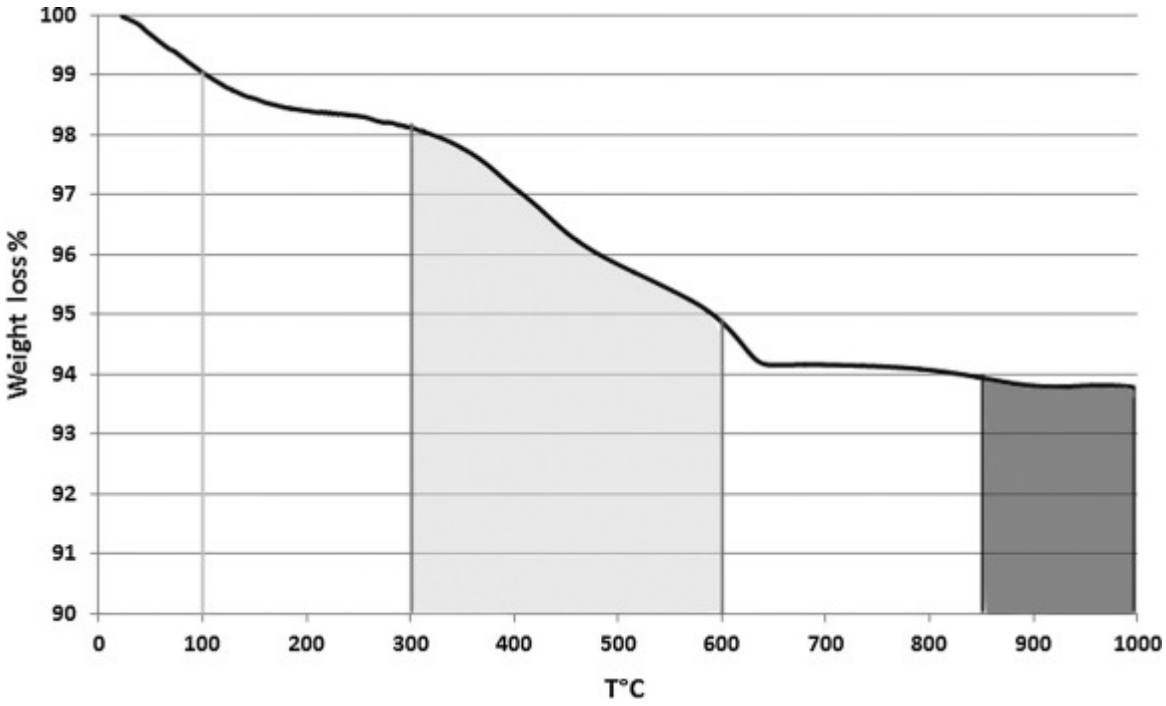

Fig. 5. Weight loss % versus T°C, from 100 up to 1000 °C of a subsample representative of the grain size distribution of bottom ashes.

This is the authors copy of the original published in https://doi.org/10.1016/j.wasman.2018.11.050

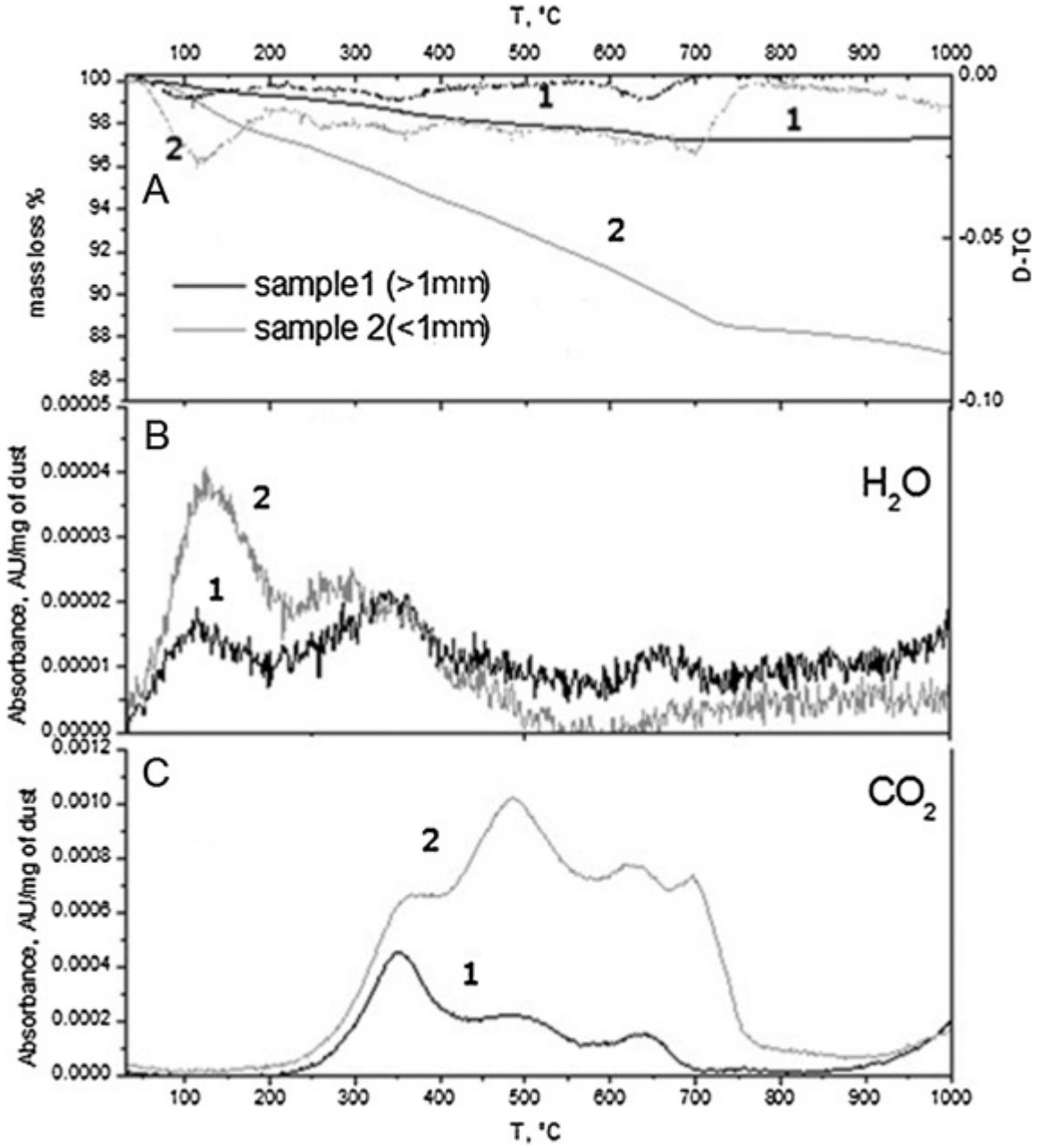

Fig. 6. TGA-FTIR analysis of the BA samples 1 and 2, characterized by grain size >1 mm and <1 mm, respectively. (A): TGA(solid line) and derivative (D-TG, dotted line) curves of sample 1 and 2 heated from 30 to 1000 °C at 20 °C min−1 under oxidizing atmosphere (O2:N2 1:3); (B): FTIR profile of the H2O evolved during the heating obtained from the variation of the absorbance at 1650 cm−1, (C): FTIR profile of the CO2 evolved during the heating obtained from the variation of the absorbance at 2360 cm−1.

This is the authors copy of the original published in https://doi.org/10.1016/j.wasman.2018.11.050

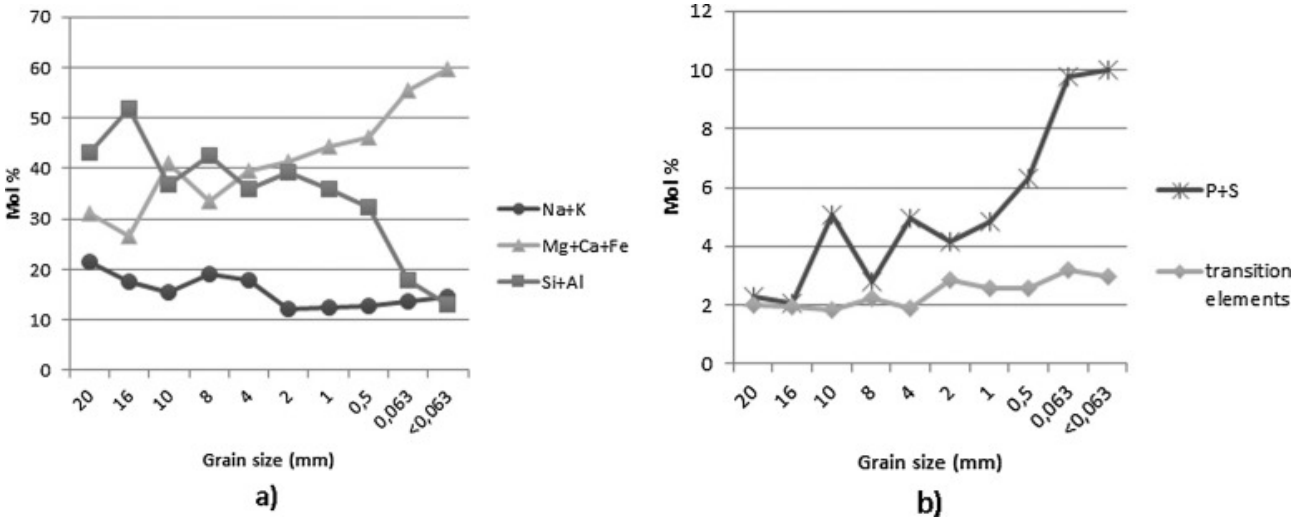

Fig. 7. a and b. Amorphous phase aggregate compositions (mol %), as function of the particle size.

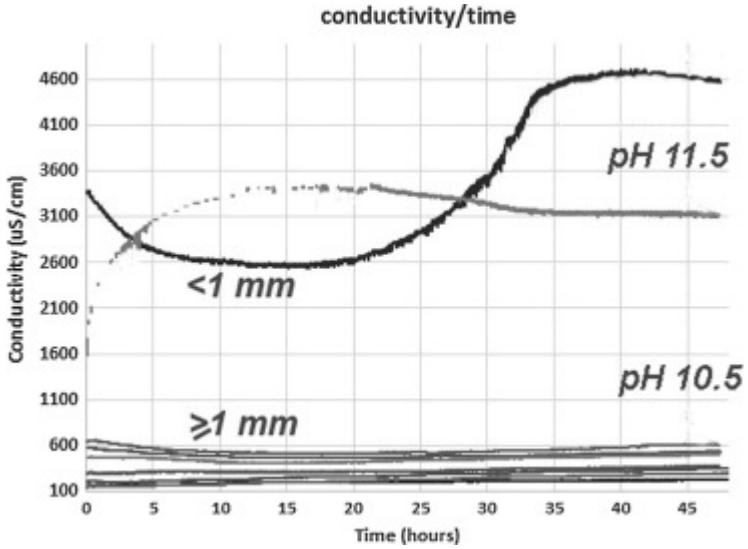

Fig. 8. Electrolytic conductivity (µS/cm) versus time (hours) during the leaching tests, for every grain size of BA. Grain size <0,063 is not reported in the diagram

This is the authors copy of the original published in https://doi.org/10.1016/j.wasman.2018.11.050

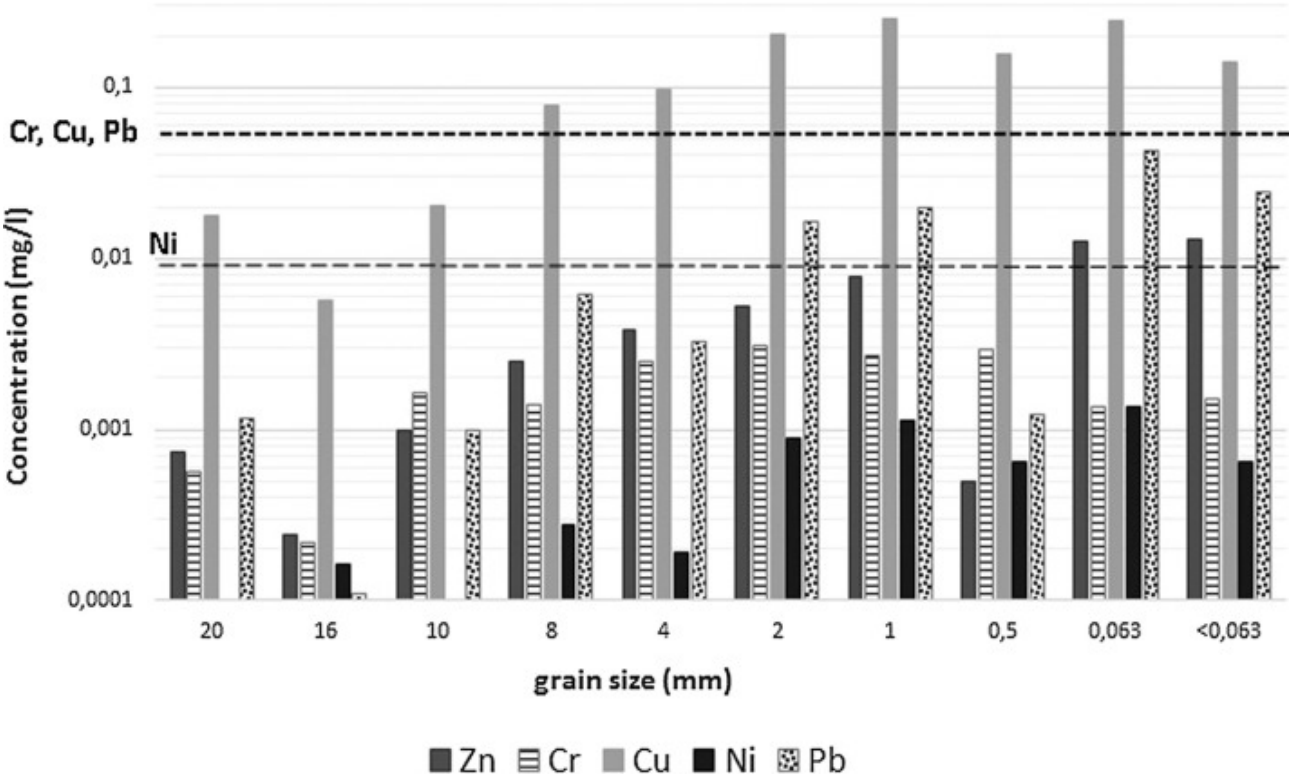

Fig. 9. Released heavy metals from BA in leaching solutions, measured by ICP-OES. Higher concentrations in the fine grain size classes than in the coarse grain size ones. Dashed lines are the legal thresholds (D.M. 5/4/2006n. 186): 0,05 mg/l for Pb, Cu, Cr and 0,01 mg/l for Ni. Co, Cd, Ba and Zn are always below the legal threshold values.

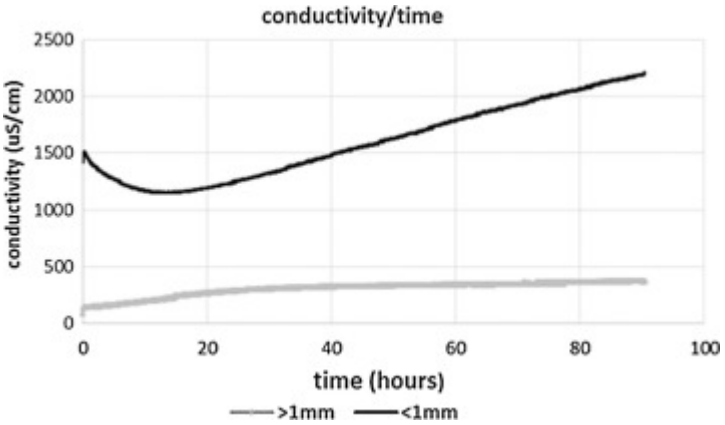

Fig. 10. Electrolytic conductivity (µS/cm) versus time (hours) during the leaching tests, for grain size ≥1 mm and <1 mm of BA.

This is the authors copy of the original published in https://doi.org/10.1016/j.wasman.2018.11.050

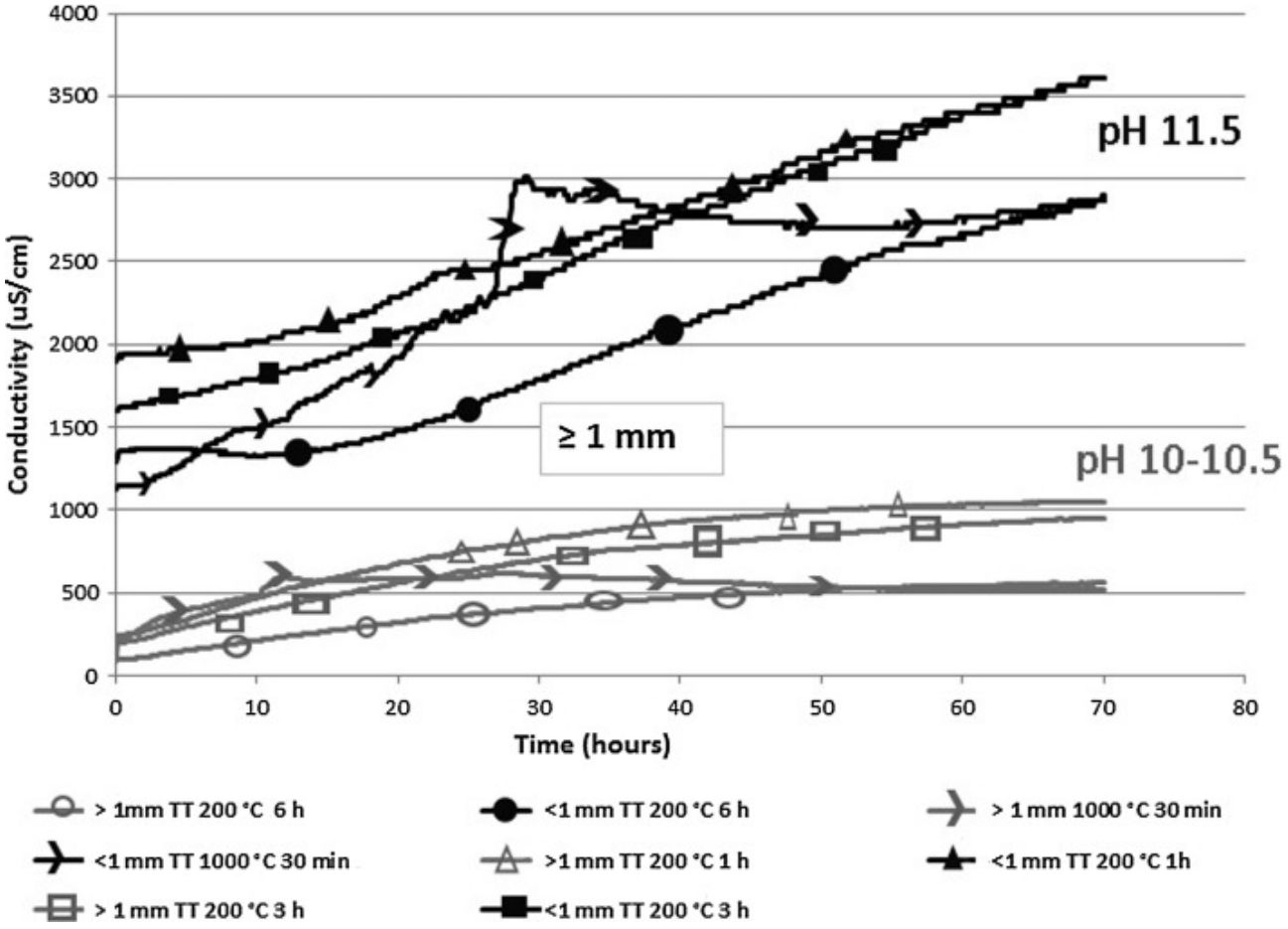

Fig. 11. Electrolytic conductivity (µS/cm) versus time (hours) during the leaching tests, for grain size ≥1 mm and <1 mm of BA, after thermal treatments at 200 °C (1, 3, 6 h) and 1000 °C (30 min). pH-values are reported for the two fractions of material.

This is the authors copy of the original published in https://doi.org/10.1016/j.wasman.2018.11.050

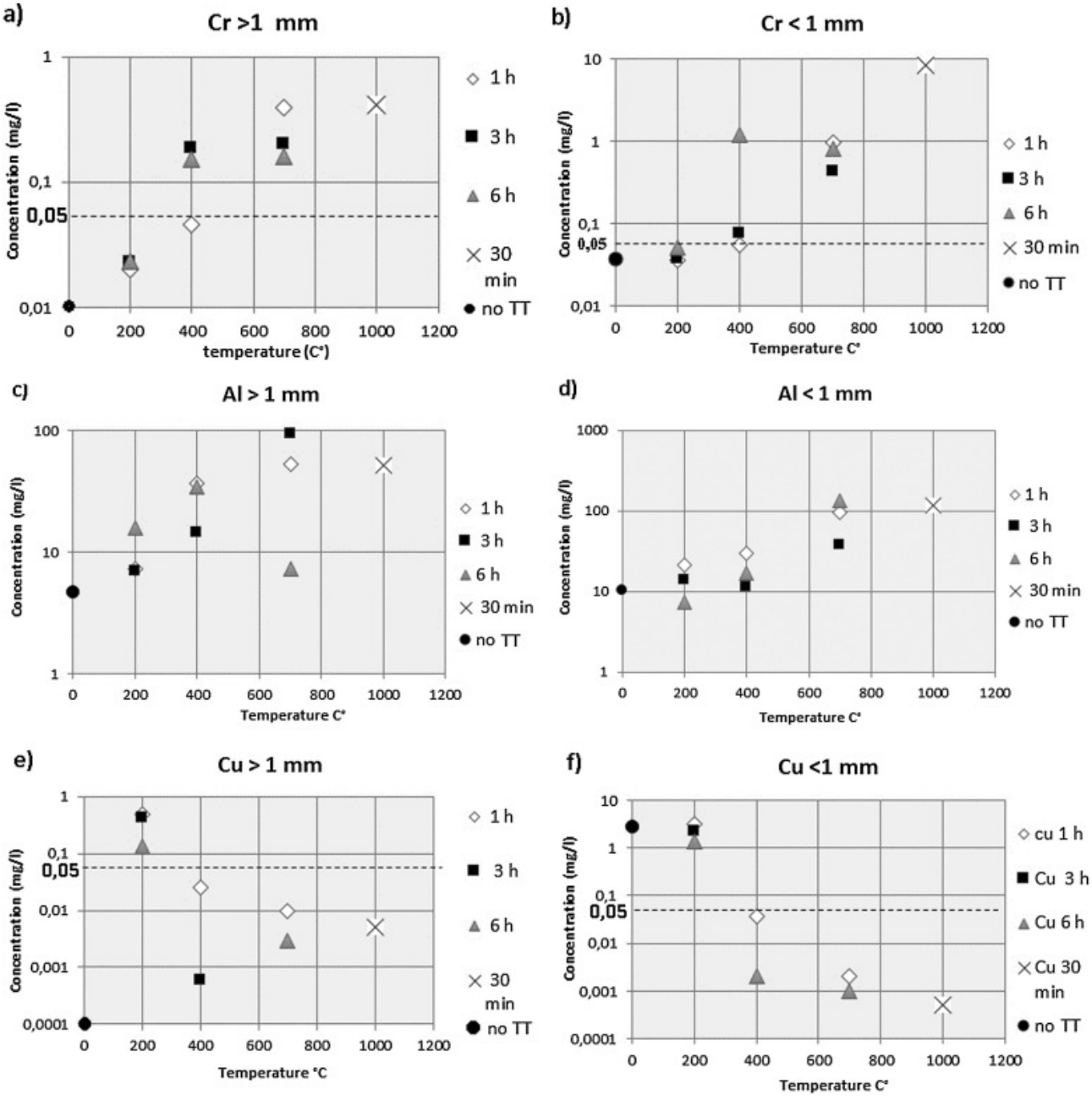

Fig. 12. a–f. Concentrations (log-scale) of Cr, Al and Cu in BA samples: no tt (no thermal treatment); treatment temperatures and times are shown. Al and Cr increase monotonically as a function of temperature, whereas Cu decreases. Dashed lines are threshold limits of law (D.M. 5/4/2006 n. 186): 0,05 mg/l for Cu and Cr. Al has no threshold limit.

This is the authors copy of the original published in https://doi.org/10.1016/j.wasman.2018.11.050

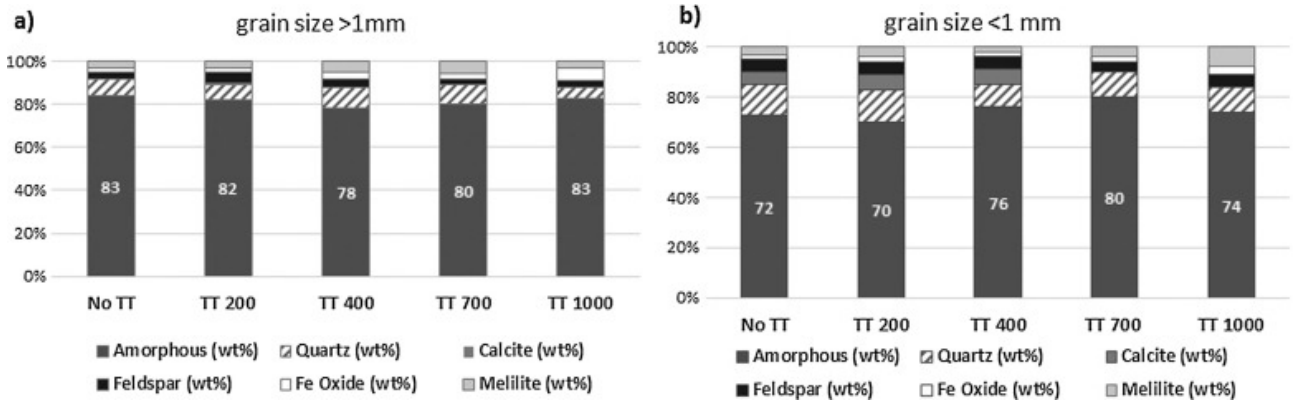

Fig. 13. a and b: XRD analysis of the BA grain size classes ≥1 and <1 mm, respectively. No TT: no thermal treatment. Figures on the histogram indicate amorphous phase content, in wt%.

References

Arickx et al., 2007

S. Arickx, T. Van Gerven, T. Knaepkens, K. Hindrix, R. Evens, C. Vandecasteele Influence of treatment techniques on Cu leaching and different organic fractions in MSWI bottom ash leachate Waste Manage., 27 (10) (2007), pp. 1422-1427

Astrup et al., 2005

T. Astrup, C. Rosenblad, S. Trapp, T.H. Christensen Chromium release from waste incineration air-pollution-control residues Environ. Sci. Technol., 2005 (39) (2005), pp. 3321-3329

Barbieri et al., 2000

L. Barbieri, A. Corradi, I. Lancellotti Bulk and sintered glass-ceramics by recycling municipal incinerator bottom ash J. Eur. Ceram. Soc., 20 (10) (2000), pp. 1637-1643

Bernasconi et al., 2018

A. Bernasconi, M. Dapiaggi, J. Wright, S. Ceola, S. Maurina, F. Francescon, A. Pavese High temperature investigation of SiO2-Al2O3-ZnO-Na2O glass for ceramic glaze: in-situ/ex-situ synchrotron diffraction and conventional approaches Ceram. Int., 44 (2018), pp. 6395-6401

Bethanis et al., 2002

S. Bethanis, C.R. Cheeseman, C.J. Sollars Properties and microstructure of sintered incinerator bottom ash

Ceram. Int., 28 (8) (2002), pp. 881-886

CEWEP, 2006

CEWEP, 2006. Environmentally sound use of bottom ash. <http://www.devon.gov.uk/text/appendix-19-cewep-environmentally-sound-use-of-bottom-ash.pdf>.

CEWEP, 2014

CEWEP, 2014. Bottom ash fact sheet. <http://www.cewep.eu/wp-content/uploads/2017/09/FINAL-Bottom-Ash-factsheet.pdf>.

Cheeseman et al., 2003

This is the authors copy of the original published in https://doi.org/10.1016/j.wasman.2018.11.050

C.R. Cheeseman, S. Monteiro da Rocha, C. Sollars, S. Bethanis, A.R. Boccaccini Ceramic processing of incinerator bottom ash Waste Manage., 23 (10) (2003), pp. 907-916

Chen et al., 2008

C.K. Chen, C. Lin, L.C. Wang, Y.C. Lin, G.P. Chang-Chien Size distribution of metals in bottom ash of municipal solid waste incinerators J. Environ. Eng. Manage., 18 (2) (2008), pp. 105-113

Chimenos et al., 2003

J.M. Chimenos, A.I. Fernandez, L. Miralles, M. Segarra, F. Espiell Short-term natural weathering of MSWI bottom ash as a function of particle size Waste Manage., 23 (10) (2003), pp. 887-895

Chimenos et al., 1999

J.M. Chimenos, M. Segarra, M.A. Fernández, F. Espiell Characterization of the bottom ash in municipal solid waste incinerator J. Hazard. Mater., 64 (1999), pp. 211-222

Cornelis et al., 2006

G. Cornelis, T. Van Gerven, C. Vandecasteele Antimony leaching from uncarbonated and carbonated MSWI bottom ash J. Hazard. Mater., 137 (3) (2006), pp. 1284-1292

Crillesen and Skaarup, 2006

Crillesen, K., Skaarup, J., 2006. Management of bottom ash from WTE plants, ISWA-WG Thermal Treatment, Subgroup Bottom Ash from WTE-Plants, pp. 34–49.

Del Valle-Zermeño et al., 2017

R. Del Valle-Zermeño, J. Gómez-Manrique, J. Giro-Paloma, J. Formosa, J.M. Chimenos Material characterization of the MSWI bottom ash as a function of particle size. Effects of glass recycling over time Sci Total Environ., 581–582 (2017), pp. 897-905

De Windt et al., 2011

L. De Windt, D. Dabo, S. Lidelöw, R. Badreddine, A. Lagerkvist MSWI bottom ash used as basement at two pilot-scale roads: comparison of leachate chemistry and reactive transport modelling Waste Manage. Environ. Implicat. Alternative Mater. Construct. Treat. Waste, 31 (2) (2011), pp. 267-280

Dou et al., 2017

X. Dou, F. Ren, M.Q. Nguyen, A. Ahamed, K. Yin, W.P. Chan, V.W.C. Chang Review of MSWI bottom ash utilization from perspectives of collective characterization, treatment and existing application Renew. Sustain. Energy Rev., 79 (2017), pp. 24-38

Eusden et al., 1999

J.D. Eusden, T.T. Eighmy, K. Hockert, E. Holland, K. Marsella Petrogenesis of municipal solid waste combustion bottom ash Appl. Geochem., 14 (1999), pp. 1073-1091

Eymael et al., 1994

Eymael MT, De Wijs W, Mahadew D., 1994. The Use of MSWI Bottom Ash in Asphalt Concrete. In: Goumans, J.J.J.M. van der Sloot, H.A., Aalbers, Th. G. (Eds.), Studies in Environmental Science, Elsevier, 60, pp. 851–862. Environmental Aspects of Construction with Waste Materials.

Forteza et al., 2004

This is the authors copy of the original published in https://doi.org/10.1016/j.wasman.2018.11.050

R. Forteza, M. Far, C. Segui, V. Cerda Characterization of bottom ash in municipal solid waste incinerators for its use in road base Waste Manage., 24 (2004), pp. 899-909

Gerlach et al., 2002

R.W. Gerlach, D.E. Dobb, G.A. Raab, J.M. Nocerino Gy sampling theory in environmental studies. 1. Assessing soil splitting protocols J. Chemometrics, 16 (7) (2002), pp. 321-328

Grygar et al., 2004

T. Grygar, T. Rojka, P. Bezdička, E. Večerníková, F. Kovanda Voltammetric and X-ray diffraction analysis of the early stages of the thermal crystallization of mixed Cu, Mn oxides J Solid State Electrochem., 8 (2004), pp. 252-259

Grosso et al., 2011

Grosso M., Rigamonti M., Biganzoli L., 2011. Italian experience and research on bottom ash recovery. "From ashes to metals", CEWEP – EAA Seminar 5th – 6th September 2011, Copenhagen.

Gualtieri, 2000

A. Gualtieri Accuracy of XRPD QPA using the combined Rietveld-RIR method" J. Appl. Cryst., 33 (2000), pp. 267-278

Hjelmar and Holm, 2007

O. Hjelmar, J. Holm, K. Crillesen Utilisation of MSWI bottom ash as sub-base in road construction: First results from a large-scale test site J. Hazard. Mater., First Int. Conf. Eng. Waste Treatment: Beneficial Use of Waste By-Products (WasteEng2005), 139 (3) (2007), pp. 471-809

Huang et al., 2006

C.M. Huang, W.F. Yang, H.W. Ma, Y.R. Song The potential of recycling and reusing municipal solid waste incinerator ash in Taiwan Waste Manage., 26 (9) (2006), pp. 979-987

Hyks et al., 2010

J. Hyks, I. Nesterov, E. Mogensen, P.A. Jensen, T. Astrup Leaching from waste incineration bottom ashes treated in a rotary kiln Waste Manage. Res., 29 (10) (2011), pp. 995-1007

ISPRA, 2017

ISPRA – Istituto Superiore per la Protezione e la Ricerca Ambientale. 2017. Rapporto rifiuti urbani. Edizione 2017. ISPRA Rapporti 272/2017.

ISPRA, 2014

ISPRA – Istituto Superiore per la Protezione e la Ricerca Ambientale. (2014). Rapporto sul recupero energetico da rifiuti urbani in Italia. ISPRA Rapporti 209/2014.

Izquierdo et al., 2002

M. Izquierdo, A. López-Soler, E. Vazquez, M. Barra, X. Querol Characterisation of bottom ash from municipal solid waste incineration in Catalonia J. Chem. Technol. Biotechnol., 77 (2002), pp. 576-583

Jung et al., 2004

C.H. Jung, T. Matsuto, N. Tanaka, T. Okada Metal distribution in incineration residues of municipal solid waste (MSW) in Japan Waste Manage., 24 (4) (2004), pp. 381-391
This is the authors copy of the original published in https://doi.org/10.1016/j.wasman.2018.11.050

Lam et al., 2010

C.H.K. Lam, A.W.M. Ip, J.P. Barford, G. McKay Use of incineration MSW Ash: a review Sustainability, 2 (7) (2010), pp. 1943-1948

Le et al., 2018

N.H. Le, A. Razakamanantsoa, M.L. Nguyen, V.T. Phan, P.L. Dao, D.H. Nguyen Evaluation of physicochemical and hydromechanical properties of MSWI bottom ash for road construction Waste Manage., 80 (2018), pp. 168-174

Lin et al., 2017

W.Y. Lin, K.S. Heng, M.Q. Nguyen, J.R.I. Ho Evaluation of the leaching behavior of incineration bottom ash using seawater: a comparison with standard leaching tests Waste Manage., 62 (2017), pp. 139-146

Lombardi and Carnevale, 2016

L. Lombardi, E.A. Carnevale Bottom ash treatment at the site of producing plant for reutilization Waste Biomass Valorization, 7 (2016), pp. 965-974

Lothenbach et al., 2011

B. Lothenbach, K. Scrivener, R.D. Hooton Supplementary cementitious materials Cem. Concr. Res., 41 (2011), pp. 1244-1256

Lynn et al., 2017

C.J. Lynn, G.S. Ghataora, O.B.E.R.K. Dhir Municipal incinerated bottom ash (MIBA) characteristics and potential for use in road pavements Int. J. Pavement Res. Technol., 10 (2) (2017), pp. 185-201

Marinoni et al., 2017

N. Marinoni, V. Diella, G. Confalonieri, A. Pavese, F. Francescon Soda-Lime-Silica-glass/quartz particle size and firing time: their combined effect on sanitary-ware ceramic reactions and macroscopic properties Ceram. Int., 43 (2017), pp. 10895-10904

Marinoni et al., 2013

N. Marinoni, D. D'Alessio, V. Diella, A. Pavese, F. Francescon Effects of soda- lime- silica waste glass on mullite formation kinetics and micro-structures development in vitreous ceramics J. Environ. Manage., 124 (2013), pp. 100-107

Marinoni et al., 2009

N. Marinoni, M. Voltolini, L. Mancini, P. Vignola, A. Pagani, A. Pavese An investigations of mortars affected by alkali-silica reaction by X-ray synchrotron microtomography: a preliminary study J. Mater. Sci., 44 (2009), pp. 5815-5823

Matsuzawa et al., 2006

Y. Matsuzawa, K. Mae, S. Kitano, S. Yoshihara, S. Ueno, J. Nishino, N. Kubota Leaching behavior of heat-treated waste ash Fuel, 85 (2006), pp. 401-409

Miezah et al., 2015

This is the authors copy of the original published in https://doi.org/10.1016/j.wasman.2018.11.050

K. Miezah, K. Obiri-Danso, Z. Kadar, B. Fei-Baffoe, M.Y. Mensah Municipal solid waste characterization and quantification as a mesure towards effective waste management in Ghana Waste Manage., 46 (2015), pp. 15-27

Minane et al., 2017

Minane, J.R., Becquart, F., Abriak, N.E., Deboffe, C., 2017. Upgraded Mineral Sand Fraction from MSWI Bottom Ash: An Alternative Solution for the Substitution of Natural Aggregates in Concrete Applications. Procedia Engineering, International High-Performance Built Environment Conference – A Sustainable Built Environment Conference 2016 Series (SBE16), iHBE 2016, 180, n. Supplement C.

Ministero dell'Ambiente, 2006

Ministero dell'Ambiente e della Tutela del Territorio, 2006. Decreto 5 aprile 2006, n.186. Regolamento recante modifiche al decreto ministeriale 5 febbraio 1998 «Individuazione dei rifiuti non pericolosi sottoposti alle procedure semplificate di recupero, ai sensi degli articoli 31 e 33 del decreto legislativo 5 febbraio 1997, n. 22». Gazzetta Ufficiale N. 115 ,19 Maggio 2006.

Møller, 2004

H. Møller Sampling of heterogeneous bottom ash from municipal waste-incineration plants Chemomet. Intel. Lab. Syst., 74 (2004), pp. 171-176

European Union, 2017

European Union, 2017. Council Regulation (EU) 2017/997 of 8 June 2017 amending Annex III to Directive 2008/98/EC of the European Parliament and of the Council as regards the hazardous property HP 14 'Ecotoxic' (Text with EEA relevance). OJ L 150, pp. 1–4.

Pagani et al., 2010

A. Pagani, F. Francescon, A. Pavese, V. Diella Sanitary-ware vitreous body characterization method by optical microscopy, elemental maps, image processing and X-ray powder diffraction J. Eur. Ceram. Soc., 30 (6) (2010), pp. 1267-1275

Palmer et al., 2005

Palmer, D.A., Benezeth, P., Simonson, J.M., 2005. Solubility of copper oxides in water and steam. In: M. Nakahara, N. Matubayasi, M. Ueno, K. Yasuoka, K. Watanabe (Eds.). Water, steam and aqueous solutions for electric power: advances in science and technology. Proc. 14th Int. Conf. on the Properties of Water and Steam, 29 August–3 September 2003, Kyoto, Japan, pp. 491-496

Pan et al., 2008

J.R. Pan, C. Huang, J.J. Kuo, S.H. Lin Recycling MSWI bottom and fly ash as raw materials for portland cement Waste Manage., 28 (2008), pp. 1113-1118

Petersen et al., 2005

L. Petersen, P. Minkkinen, K.H. Esbensen Representative sampling for reliable data analysis: theory of Sampling Chemomet. Intell. Lab. Syst., 77 (2005), pp. 261-277

Puma et al., 2013

S. Puma, F. Marchese, A. Dominijanni, M. Manassero Reuse of MSWI bottom ash mixed with natural sodium bentonite as landfill cover material Waste Manage. Res., 31 (6) (2013), pp. 577-584

This is the authors copy of the original published in https://doi.org/10.1016/j.wasman.2018.11.050

Quina et al., 2008

M.J. Quina, J.C. Bordado, R.M. Quinta-Ferreira Treatment and use of air pollution control residues from MSW incineration: an overview Waste Manage., 28 (2008), pp. 2097-2121

Riva et al., 2016

A. Riva, L. Biganzoli, M. Grosso Gestione delle scorie da incenerimento di rifiuti solidi urbani: sistemi di estrazione e layout impiantistici di trattamento Ingegneria dell'Ambiente, 3 (1) (2016), pp. 28-42

Schabbach et al., 2012

L.M. Schabbach, G. Bolelli, F. Andreola, I. Lancellotti, L. Barbieri Valorization of MSWI bottom ash through ceramic glazing process: a new technology J. Cleaner Prod., 23 (2012), pp. 147-157

Shih and Ma, 2011

H.C. Shih, H. Ma Assessing the health risk of reuse of bottom ash in road paving Chemosphere, 82 (11) (2011), pp. 1556-1562

Shim et al., 2003

Y.S. Shim, Y.K. Kim, S.H. Kong, S.W. Rhee, W.K. Lee The adsorption characteristics of heavy metals by various particle sizes of MSWI bottom ash Waste Manage., 23 (9) (2003), pp. 851-857

Smol et al., 2015

M. Smol, J. Kulczycka, A. Henclik, K. Gorazda, Z. Wzorek The possible use of sewage sludge ash (SSA) in the construction industry as a way towards a circular economy J. Cleaner Prod., 95 (2015), pp. 45-54

Sorlini et al., 2011

S. Sorlini, A. Abbà, C. Collivignarelli Recovery of MSWI and soil washing residues as concrete aggregates Waste Manage., 31 (2) (2011), pp. 289-297

Toby and Von Dreele, 2013

B.H. Toby, R.B. Von Dreele GSAS-II: the genesis of a modern open-source all purpose crystallography software package J. Appl. Cryst., 46 (2) (2013), pp. 544-549

Toniolo and Boccaccini, 2017

N. Toniolo, A.R. Boccaccini Fly ash-based geopolymers containing added silicate waste. A review Ceram. Int., 43 (2017), pp. 14545-14551

Tsakalou et al., 2018

C. Tsakalou, S. Papamarkou, P.E. Tsakiridis, G. Bartzas, K. Tsakalakis Characterization and leachability evaluation of medical wastes incineration fly and bottom ashes and their vitrification outgrowths J. Environ. Chem. Eng., 6 (2018), pp. 367-376

Van Caneghem et al., 2016

J. Van Caneghem, B. Verbinnen, G. Cornelis, J. de Wijs, R. Mulder, P. Billen, C. Vandecasteele Immobilization of antimony in waste-to-energy bottom ash by addition of calcium and iron containing additives Waste Manage., 54 (2016), pp. 162-168

Van Gerven et al., 2004

This is the authors copy of the original published in https://doi.org/10.1016/j.wasman.2018.11.050

T. Van Gerven, K. Imbrechts, E. Van Keer, M. Jaspers, G. Wauters, C. Vandecasteele Investigation of washing, heating and carbonation as treatment techniques for the improvement of environmental characteristics of MSWI-bottom ash in view of recycling C.A. Brebbia, S. Kungolos, V. Popov, H. Itoh (Eds.), Waste Management and the Environment II, Rhodes Greece (2004), pp. 3-12

Van Gerven et al., 2005

T. Van Gerven, E. Van Keer, S. Arickx, M. Jaspers, G. Wauters, C. Vandecasteele Carbonation of MSWI-bottom ash to decrease heavy metal leaching in view of recycling Waste Manage., 25 (3) (2005), pp. 291-300

Verbinnen et al., 2017

B. Verbinnen, P. Billen, J. Van Caneghem, C. Vandecasteele Recycling of MSWI Bottom Ash: a review of chemical barriers, engineering applications and treatment technologies Waste Biomass Valorization, 8 (2017), pp. 1453-1466

Yin et al., 2017

K. Yin, W.P. Chan, X. Dou, F. Ren, V.W.C. Chang Measurements, factor analysis and modeling of element leaching from incineration bottom ashes for quantitative component effects J. Cleaner Prod., 165 (2017), pp. 477-490

Xia et al., 2017

Y. Xia, P. He, L. Shao, H. Zhang Metal distribution characteristic of MSWI bottom ash in view of metal recovery J. Environ. Sci. (China), 52 (2017), pp. 178-189

Xiao et al., 2008

Y. Xiao, M. Oorsprong, Y. Yang, J.H. Voncken Vitrification of bottom ash from a municipal solid waste incinerator Waste Manage., 28 (6) (2008), pp. 1020-1026

This is the authors copy of the original published in https://doi.org/10.1016/j.wasman.2018.11.050